

Organic & Biomolecular Chemistry

Accepted Manuscript



This is an *Accepted Manuscript*, which has been through the Royal Society of Chemistry peer review process and has been accepted for publication.

Accepted Manuscripts are published online shortly after acceptance, before technical editing, formatting and proof reading. Using this free service, authors can make their results available to the community, in citable form, before we publish the edited article. We will replace this *Accepted Manuscript* with the edited and formatted *Advance Article* as soon as it is available.

You can find more information about *Accepted Manuscripts* in the [Information for Authors](#).

Please note that technical editing may introduce minor changes to the text and/or graphics, which may alter content. The journal's standard [Terms & Conditions](#) and the [Ethical guidelines](#) still apply. In no event shall the Royal Society of Chemistry be held responsible for any errors or omissions in this *Accepted Manuscript* or any consequences arising from the use of any information it contains.

Chromane Helicity Rule – Scope and Challenges Based on ECD Study of Various Trolox Derivatives

Marcin Górecki,^{*a} Agata Suszczyńska,^a Magdalena Woźnica,^a Aneta Baj,^b Michał Wolniak,^c
 Michał K. Cyrański,^d Stanisław Witkowski,^b and Jadwiga Frelek,^{*a}

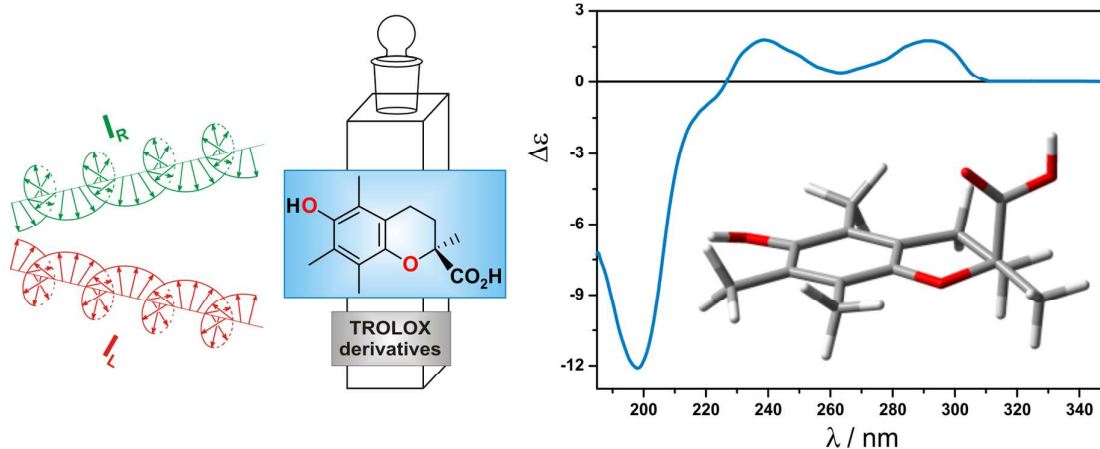
^a *Institute of Organic Chemistry, Polish Academy of Sciences, Kasprzaka 44/52, 01-224 Warsaw, Poland*

^b *University of Białystok, Institute of Chemistry, Piłsudskiego 11/4, 15-443 Białystok, Poland*

^c *Medical University of Warsaw, Faculty of Pharmacy, Department of Physical Chemistry, Banacha 1, 02-097 Warsaw, Poland*

^d *University of Warsaw, Department of Chemistry, Pasteura 1, 02-093 Warsaw, Poland*

E-mail of corresponding author: jadwiga.frelek@icho.edu.pl



ABSTRACT

The validity of the chromane helicity rule correlating the sense of twist within the dihydropyran ring with the CD sign of the 1L_b band observed at *ca.* 290 nm in their electronic circular dichroism (ECD) spectra is examined using a set of natural (*S*)-trolox derivatives. To investigate both the scope and the limitations of the rule a combination of the ECD spectroscopy, especially the temperature dependence of the ECD spectra, single crystal X-ray

diffraction analyses, and the density functional theory (DFT) calculations were used. A thorough conformational analysis supported by the X-ray data led to the identification of predominant conformers. Then, a comparison of the experimental ECD spectra with the spectra simulated by TDDFT calculations allowed for a reasonable interpretation of the accumulated data. The results clearly indicated that to avoid the possibility of erroneous conclusions the chromane helicity rule should be used with a great caution. This is likely related to the conformational flexibility of tested compounds by which conformers of different helicities can be produced. Therefore, based on the results presented here, it is strongly recommended supporting the conclusions derived from analysis of experimental data with the appropriate theoretical computations.

INTRODUCTION

Natural products containing the chromane motif very often exhibit biological activity, which is strongly dependent on the stereochemistry of the chromane unit as well as the presence of the phenolic OH group at C-6 position.^{1, 2} The most prominent example of such biologically active natural product is the vitamin E family, exemplified by, most notably, the α -tocopherol (**i**) the structure of which is shown below (Chart 1).

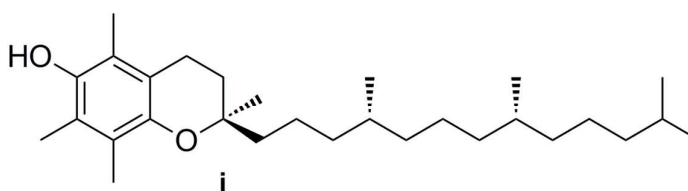


Chart 1.

α -Tocopherol is the most biologically active component of vitamin E, and it is also one of the best-known chain-breaking phenolic antioxidants.³⁻⁵ Furthermore, it stabilizes the lipid bilayers *via* van der Waals interaction with unsaturated fatty acid chains of phospholipids.⁵⁻⁷ More recent findings have also shown the involvement of vitamin E in cell signalling^{8, 9} and gene expression.^{10, 11} Additionally, there is evidence that α -tocopherol

modulates the activity of certain transcription factors, and activity of numerous enzymes.^{12, 13} Moreover, vitamin E and related analogues play an essential role in daily life, because of their biological activity and antioxidant properties.¹⁴ A specific pharmaceutical use of vitamin E such as a potential prevention of Alzheimer's and Parkinson's diseases, certain types of cancer, and many illnesses caused by oxidative stress, including the so-called lifestyle diseases can be mentioned in this context.¹⁵ Considering this wide variety of biological effects, it is not surprising that many research groups are involved not only in efforts directed at isolation and synthesis of new chromane systems but also in attempts of correlating their molecular structure with biological as well as optical activity.¹⁶⁻²⁰

For many years, the relationship between the stereostructure of chromanes and their ECD spectra was determined almost exclusively by the empirical chromane helicity rule.²¹⁻²³ This rule, developed by Snatzke *et al.*,²² binds the sign of the long-wavelength ECD band related to 1L_b excitation of the chromane chromophore, found at around 270-290 nm, with the helicity of the dihydropyran ring, as shown in Figure 1.

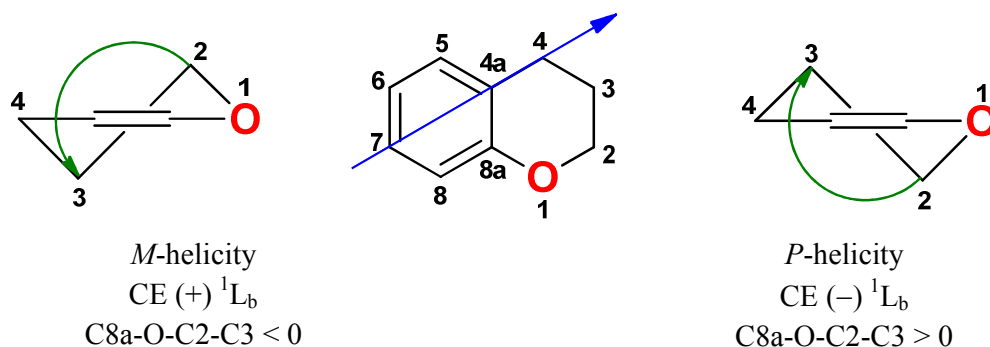


Figure 1. Graphical representation of the chromane helicity rule showing correlation between the P/M -helicity of the dihydropyran ring and the sign of the 1L_b ECD band. The approximate direction of the electric dipole transition moment vector (μ) is represented by the straight blue arrow.

According to the rule, for compounds with P -helicity of the heterocyclic ring the 1L_b ECD band is negative, while for chromanes with M -helicity, this band is positive. An

additional requirement for the application of the rule is that the largest substituent at C-2 carbon atom preferentially should occupy an equatorial position.

Since its formulation, the chromane helicity rule has been repeatedly used as an aid in the determination of the absolute configuration of a vast range of natural and synthesized products containing chromane chromophore.²⁴⁻²⁸ However, a failure of the rule has been encountered in some cases. For example, in 2009, Batista *et al.* assigned the absolute configuration of two compounds isolated from the leaves of *Peperomia obtusifolia* using the chromane rule.²⁵ One year later, however, further studies of the same compounds by Nafie *et al.* led to the revision of previous assignment.²⁹ On the basis of DFT calculations and VCD spectroscopy, the authors demonstrated the fallacy of the requirements of equatorial positioning of bulky groups at C-2 carbon atom in the heterocyclic ring. Thereby, one of the fundamental assumptions behind the chromane helicity rule has been challenged. The authors have also shown that, irrespective of *P*- or *M*-helicity of the heterocyclic ring, the given absolute configuration leads to the same sign of the diagnostic ECD band. Ultimately, the original assignment of the absolute configuration of natural chromanes isolated from *Peperomia obtusifolia* has been revised.^{25, 29}

Considering the above reports, we concluded that the chromane helicity rule requires a thorough analysis of the scope of its validity or may even need some degree of reformulation. Thus, in the present work, we shall demonstrate our research concerning the applicability and the limitations of the chromane helicity rule. As model compounds for this study, we selected a set of trolox derivatives with known absolute configuration (Chart 2). (*S*)-Trolox (**1**) [(*S*)-6-hydroxy-2,5,7,8-tetramethylchroman-2-carboxylic acid] is a water-soluble analogue of α -tocopherol, in which the phytyl chain is replaced with carboxyl group. It is frequently used as a model compound for studies of structural features, as well as a standard for evaluation of antioxidant activity (trolox equivalent antioxidant capacity, TEAC).³⁰

The model compounds **1-7**, except *ent-1*, are of the *S*-configuration consistent with stereochemical arrangement around C-2 carbon atom of natural D- α -tocopherol. Our choice of these chromanes as models is motivated by the relative rigidity of their carbon framework and thus, in comparison to natural tocopherols, the absence of large conformational effects on the CD spectra. The lack of labile phytyl side chain facilitates and greatly reduces the computational demands at the same time preserving the main conformational features of the chromane chromophore. Moreover, absence of possible rotamers contributions significantly simplifying analysis of experimental and computational data. However, to obtain more reliable results, compounds (chromanes **8-11**) characterized by a substantial conformational flexibility of the aliphatic, nonpolar side chains at C-2 carbon atom, have been incorporated into present study. Inclusion of these compounds, despite their computationally challenging nature, has enabled a close examination of the influence of substituents characterized by a different mobility and polarity on the heterocyclic ring conformation. The absolute configuration of chromanes **8** and **10** is consistent with the *2R* absolute configuration of natural D- α -tocopherol while it is as *2S* in the chromanes **9** and **11**. This stereochemistry descriptor change follows the switch in the group priorities, following the Cahn-Ingold-Prelog sequence rules.

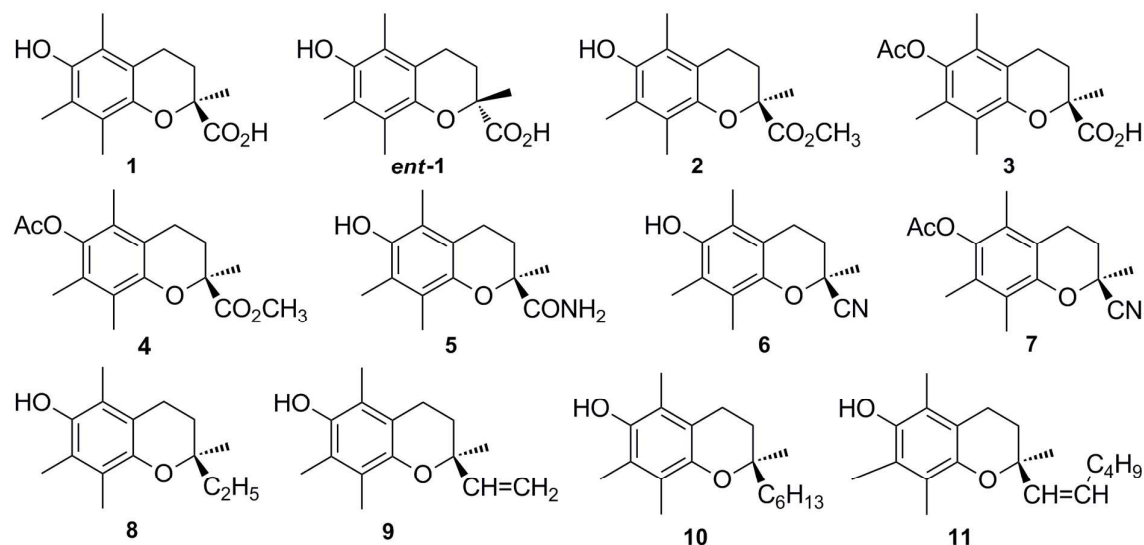


Chart 2.

We intend to gain the planned goal by scrutiny of the effect of changes of conformation of the dihydropyran ring on the diagnostic ECD bands. Our studies are focused on the band attributed to the 1L_b transition and occurring at around 290 nm because this band is the subject of the chromane helicity rule. Moreover, this ECD band is relatively distant from the next bands of higher energy that there is no danger of confusing overlapping. Thus, analysis of the long-wavelength spectral region simplifies stereochemical correlation.

To attain the desired goal, we decided to use ECD spectroscopy in tandem with time dependent density functional theory (TDDFT) calculations to support and evaluate the experimental results. It is commonly accepted that chiroptical methods combined with quantum chemical calculations are nowadays the most powerful tools for elucidating stereochemistry and monitoring even the smallest changes in the geometry of chiral molecules.³¹⁻³⁴ The comparison of experimental and theoretical CD spectra has already proven efficient and reliable for the assignment of the absolute configuration of various chiral organic molecules.³⁵⁻³⁹ To assist with achievement of the objectives of the planned study, the dependence of solvent and temperature on the ECD spectra was also used for the examination of conformational lability. Moreover, vibrational circular dichroism (VCD) was applied for selected chromans in order to obtain the most reliable results. Such a combined approach of more than one chiroptical method is widely recognized as leading to the most dependable assignment of absolute configuration.⁴⁰ In some cases, only such a treatment allows to correctly identify the three dimensional structure.^{29, 41} Furthermore, a single crystal X-ray structure determination was applied, where possible, to obtain the most accurate results.

RESULTS AND DISSCUSION

The experimental electronic absorption and chiroptical data of chromanes **1-11** are collected in Table 1. As an example, the ECD spectra of chromanes **1**, *ent-1* and **4** recorded in acetonitrile are presented in Figure 2.

The UV-vis spectra of **1-11** exhibit well-resolved absorption bands at around 290 and 200 nm with a shoulder at ~220 nm. In the context of the ECD bands intensity, however, compounds **1-11** can be divided into two groups. In the first group, containing chromanes **1-7**, the ECD spectra show quite similar profiles. They exhibit ECD absorptions at ~290 nm, attributable to the 1L_b band with a fairly intense positive CE and comparable intensities of $\Delta\epsilon \approx 1.5$. As expected, the only exception is chromane *ent-1*, which, as an enantiomer of **1**, exhibits CEs of the same intensity but opposite signs (Figure 2, left).

Another pronounced bands within this group of chromanes, characterized by moderate to strong intensity, are observed at ~240 and ~200 nm, respectively (Table 1). These ECD bands are assignable to 1L_a (~240 nm) and 1B_b (~200 nm) of $\pi\pi^*$ electronic transition of aromatic moieties, respectively, although they can overlap with other transitions such as $n\pi^*$ above 250 nm.

Table 1. UV and ECD data of chromanes **1-11** recorded in acetonitrile. UV and ECD values are given as ϵ (λ_{\max}/nm) and $\Delta\epsilon$ (λ_{\max}/nm), respectively.

Comp.	UV ϵ (λ_{\max})			ECD $\Delta\epsilon$ (λ_{\max})		
	1B_b	1L_a	1L_b	1B_b	1L_a	1L_b
1	48160 (196.0)	9680 (221.5) [#]	3150 (292.0)	-1.1 (222.5) [#] -13.0 (197.5)	+2.2 (239.5)	+1.9 (290.0)
<i>ent-1</i>	43800 (201.0)	9600 (222.0) [#]	3100 (292.5)	+1.3 (222.5) [#] +12.5 (198.0)	-2.0 (239.5)	-1.8 (291.0)
2	37050 (200.0)	9500 (222.0) [#]	3180 (292.0)	-7.6 (204.0)	+2.0 (241.5)	+1.9 (294.0) +1.9 (289.5)
3	36030 (195.0)	8740 (226.0) [#]	1800 (283.5)	-12.3 (201.0)	+3.4 (235.0)	+1.2 (282.0)
4	59550 (199.0)	10900 (222.0) [#]	1710 (284.0) 1510 (276.0)	-13.9 (206.5)	+3.2 (234.5)	+1.3 (283.5) +1.2 (277.0)
5	44700 (200.0)	10140 (223.0) [#]	2930 (293.0)	-15.9 (199.0)	+1.9 (237.5)	+1.1 (289.5)
6	37320 (201.0)	9055 (222.5) [#]	1360 (292.0) 1335 (288.0)	+8.9 (214.0)	+1.8 (239.0)	+2.5 (289.0)
7	42650 (202.0)	10250 (222.0) [#]	1250 (283.0) 1110 (275.0)	+17.9 (209.0) -17.6 (199.0)	+5.2 (227.0)	+1.8 (283.0) +1.6 (274.0)

8	40420 (197.0)	9470 (223.0) [#]	3280 (294.0)	-0.33 (214.5) [#]	+0.08 (250.5)	+0.07 (297.5) +0.05 (286.0)
9	38400 (201.0)	10020 (221.0) [#]	3040 (293.5)	-0.94 (211.0) -20.1 (194.0)	+0.07 (255.4) -0.08 (237.4)	+0.01 (310.6) -0.22 (287.6)
10	40950 (202.0)	13760 (224.0) [#]	3280 (294.0)	+1.5 (206.0) -1.0 (194.0)	+0.11 (248.0)	-0.10 (293.5) -0.09 (286.5)
11	40550 (201.5)	7820 (227.0) [#]	3090 (294.0)	+10.5 (208.5) -30.7 (196.0)	+1.63 (229.0)	+0.02 (308.5) -0.17 (296.0) -0.19 (289.0)

[#] shoulder

In the second group, consisting of chromanes **8-11**, the intensity of ECD absorption bands in the full spectral range is at least an order of magnitude weaker than those displayed by the first group. It strongly suggests the conformational flexibility of the latter chromanes. For this reason, both groups of compounds will be discussed separately. It has to be noted that other relevant data such as the positions of the ECD bands for compounds in the second group is congruent with those for the first group.

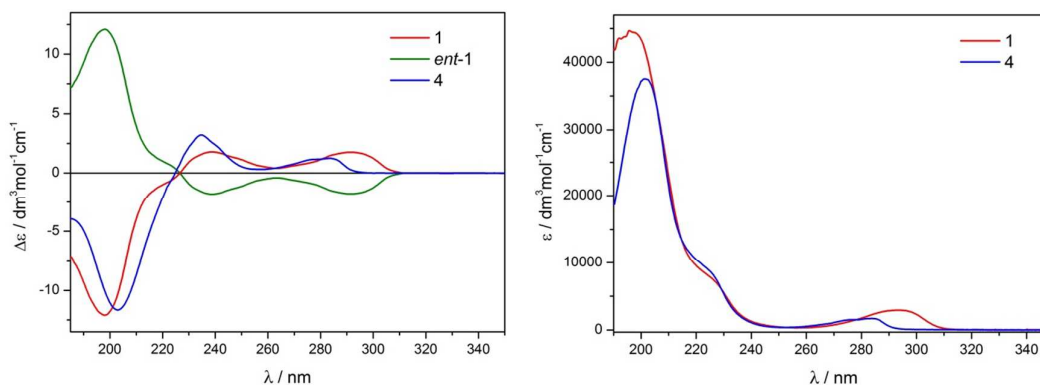


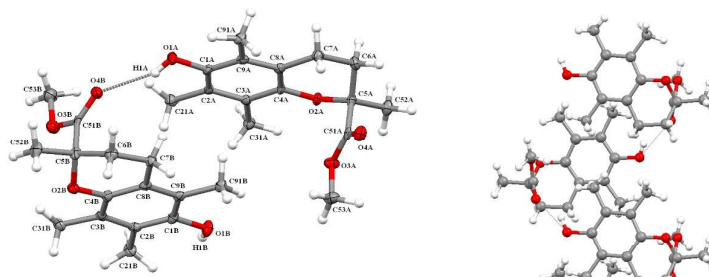
Figure 2. ECD (left) and UV (right) spectra of chromanes **1**, *ent*-**1**, and **4** recorded in acetonitrile in the 350-220 nm range. The symbol ϵ denotes the molar decadic absorption coefficient, $\Delta\epsilon$ – the difference of the molar decadic absorption coefficients of left and right circularly polarized light, and λ – the wavelength.

The similarity of the ECD curves shape, as well as practically the same intensity and location of corresponding ECD bands, clearly indicates the same conformation of the heterocyclic ring in compounds **1-7**. Nonetheless, the absorption maxima of the 1L_b band in the spectra of chromanes with an acetoxy group at C-6 (compounds **3**, **4** and **7**) are slightly blue-shifted (*ca.* 10 nm) relative to the derivatives with a hydroxyl group at the same position (compounds **1**, *ent*-**1**, **2**, and **6**). On the other hand, the ECD spectra of chromanes with

different substituents on the C-2 carbon atom show very similar profiles (Figure 2, Table 1). It implies that substituents at both the C-2 position and aromatic ring have a limited influence on ring conformation and thus have a negligible effect on the ECD curves within compounds **1-7**.

To verify the above conclusions, the conformations of chromanes **1-3**, **5** and **6** derived from a single crystal X-ray structure analysis were compared. The data for **1**,⁴² **3**,⁴² **5**,⁴³ and **6**⁴⁴ were taken from our earlier published reports, and crystallographic data for **2** are obtained in the course of this work.

(*S*)-Trolox methyl ester (**2**) crystallizes in monoclinic $P2_1$ space group with two molecules in an independent part of the unit cell. Both molecules are situated antiparallel and interact by rather strong hydrogen bond which involves hydroxyl group of one molecule (A) and the carbonyl group of the other (B). The H1A...O4B distance is found equal to 2.08(5) Å (the O1A...O4B distance equals to 2.796 (4) Å). The remaining hydroxyl or carbonyl groups of B or A molecule, respectively, form similar, albeit slightly weaker hydrogen bonds with the proximal molecules related by $[x,y,1+z]$ symmetry. In this case, the O1B-H1B...O4A is equal to 2.0(5) Å (the O1B...O4A distance equals to 2.816 (4) Å). The participating molecules are again situated antiparallel in respect to each other, what results in formation of an infinite helical chain along [001]direction (see Figure 3). There are no other strong hydrogen bond interactions in the crystal lattice, whereas the chains interact with each other by a set of rather weak CH...O or C...CH...C interactions, which range in 2.569-2.710 Å or 2.792-2.868 Å, respectively.



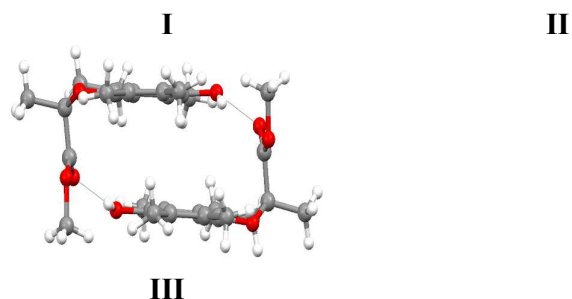


Figure 3. I: Two molecules of chromane **2** constituting an independent part of the unit cell. The displacement ellipsoids are drawn at 50 % probability level. The intermolecular hydrogen bond is marked by a dotted line; Helical chain are formed by the molecules along [001] direction; II: view along [100] direction; III: view along the [001] direction. (Note: A different numbering system is used for the structural data deposited with the CCDC.)

As can be seen in Figure 4, the X-ray crystal structures established that the dihydropyran ring in all compounds adopt the same half-chair conformation with the methyl group at C-2 in the equatorial position and the larger substituent at the same carbon atom in the axial position (Figures 3III and 4). It should be emphasized here that the comparison of size of substituents is not necessarily a simple task. Among others, a significant impact on the overall Gibbs free energy exert steric effects the differences in which largely determine the relative apparent sizes of substituents. Clearly, there are other possible stereoelectronic interactions that influence the preference of a substituent to reside either in equatorial or axial position.⁴⁵ Thus, the conformational energy does not depend simply on the size of the substituent but is a combination of several factors.. Throughout this paper, we define the size of the substituents as their van der Waals volume since it measures the steric hindrance of substituents.⁴⁶

The negative torsion angle of the C8a–O–C2–C3 unit in **1-3**, **5** and **6** corresponds to the *M*-helicity, and this is manifested in their ECD spectra by the positive 1L_b band. The axial arrangement of bulky substituent at C-2 is inconsistent with one of the fundamental requirement of chromane helicity rule.

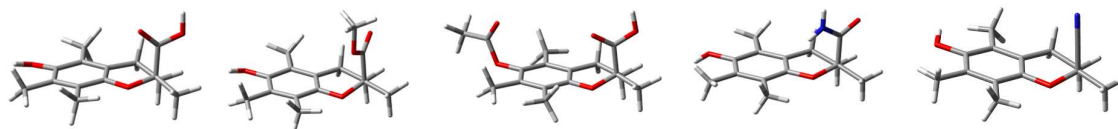


Figure 4. Comparison of solid state conformation of chromanes **1-3**, **5** and **6** derived from a single crystal X-ray structure determination.

To strengthen the conclusions regarding the conformational homogeneity of the dihydropyran ring in compounds **1-7**, the detailed conformational studies were performed. Within this part of studies, measurements of ECD spectra in various solvents and at variable temperatures were taken with chromane **2** as a representative model compound.

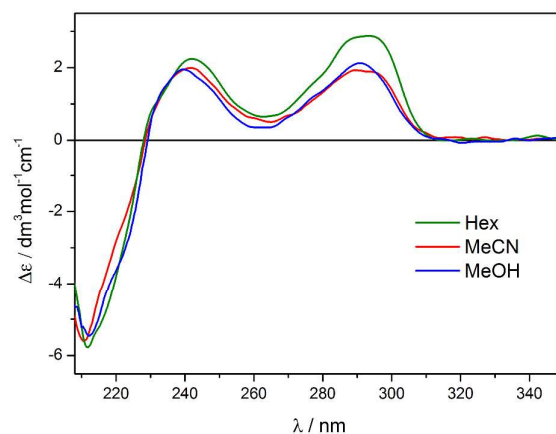


Figure 5. ECD spectra of chromane **2** recorded in various solvents at room temperature. The symbol ϵ denotes the molar decadic absorption coefficient, $\Delta\epsilon$ – the difference of the molar decadic absorption coefficients of left and right circularly polarized light, and λ – the wavelength.

In the spectra of **2** measured in acetonitrile, hexane, methanol, and chloroform no significant differences in positions of the bands and only small changes in their intensity are observed (Figure 5 and Figure S1 in SuppInfo). This clearly indicates the restricted mobility of the dihydropyran ring because a high sensitivity of the 1L_b chromane absorption to any conformational changes, including solvent effects, is well known in the literature.⁴⁷

An additional confirmation of this significant conformational homogeneity comes from ECD measurements at variable temperatures. Such a measurement made in a non-polar solvent MI₁₃ (methylcyclohexane/isopentane, 1:3, v/v) at temperatures ranging from +25 °C to –180 °C shows almost no changes in the ECD bands position and a slight increase in the intensity of the bands only. Here, the index I_{-180}^{+25} describing the relative change of $\Delta\epsilon_{\max}$ going from the low to the high temperature amounts to –11%, indicating significant

conformational stability.⁴⁸ However, for measurements recorded within the same temperature range in EPA (ethanol/isopentane/diethyl ether, 2:5:5, v/v) representing polar solvents, index I_{-180}^{+25} equal to -44% points to a greater degree of conformational freedom, nevertheless still demonstrating a noticeable hindrance to the unlimited mobility (Figure 6).⁴⁸ The result of ECD measurements *versus* temperature is in line with expectations because lowering the temperature causes progressive elimination of high-energy conformers from the equilibrium and shifts it toward the most stable conformer. In this case, such a shift means that the most stable conformation was frozen out at the lowest temperature or at least has reached a very high population. Thus, further corroboration of the relative conformational stability of the chromophoric system in chromane **2** in solution was achieved.

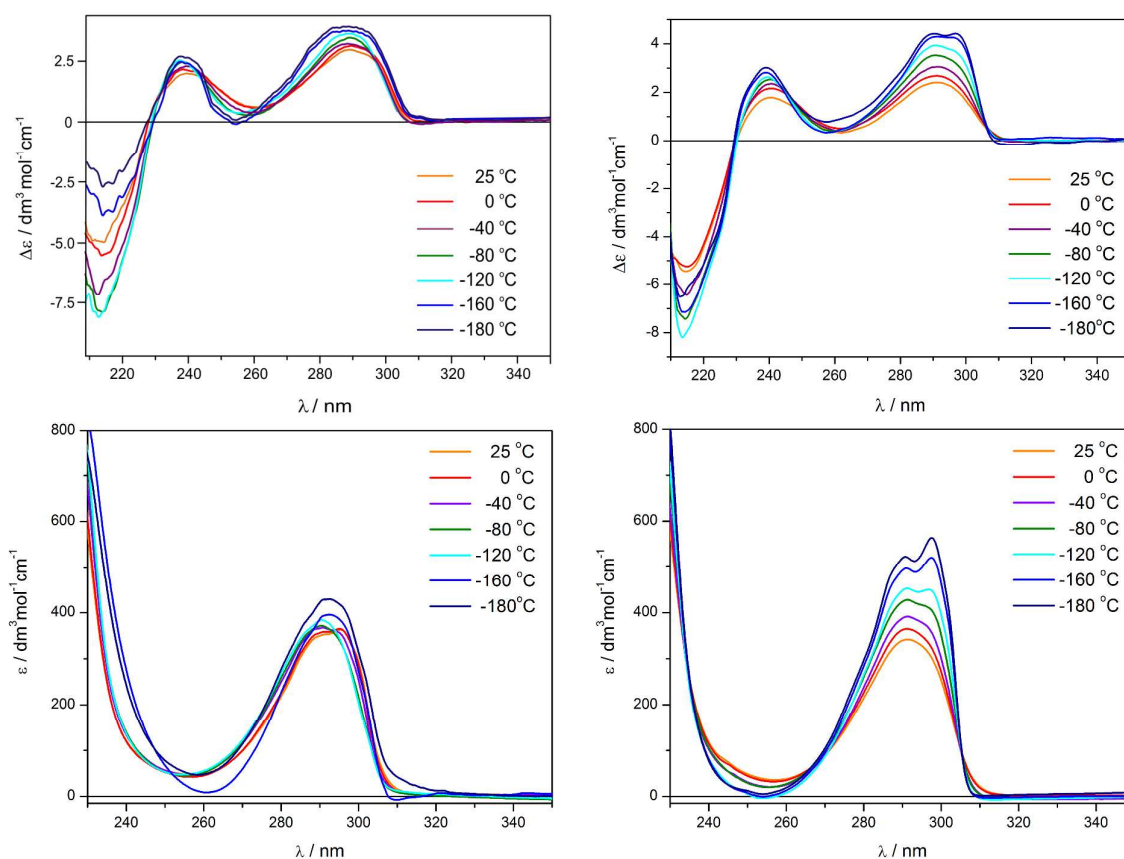


Figure 6. ECD (top) and UV-Vis (bottom) spectra of chromane **2** recorded in EPA (right) and MI_{13} (left). The symbol ε denotes the molar decadic absorption coefficient, $\Delta\varepsilon$ – the difference of the molar decadic absorption coefficients of left and right circularly polarized light, and λ – the wavelength.

To rationalize the experimental observations and to elucidate the respective contributions of possible conformers in the solution phase, the relevant calculations using molecular modelling (MM+ force field) followed by DFT optimization of resulted structures at the B3LYP/6-31G(d) level of theory were performed for **1-7**. In the next step, the simulations of the ECD spectra were conducted by means of TDDFT method using the B3LYP/6-311++G(d,p) level of theory and applying the polarizable continuum model (PCM) to reflect solvent influence.

First, the applied calculation methodology was validated by direct comparison of the geometry-related data obtained from the X-ray studies and the molecular modelling. Chromane **2** was selected as a preliminary subject for the computational procedure.

Table 2. Calculated at the B3LYP/6-31G(d) level of theory Gibbs free energy (ΔG) in kcal/mol, population (pop) at 25 °C in %, C8a–O–C2–C3 torsion angle in deg (°) and calculated ECD signs of the 1L_b ECD band of chromane **2** conformers. Atom numbering as in Figure 1.

Conf.	ΔG	Pop.	C8a–O–C2–C3	Helicity	ECD sign of 1L_b band
2a	0.0	83.4	–49.8	<i>M</i>	+
2b	1.0	15.8	–47.3	<i>M</i>	+
2c	2.7	0.8	+47.5	<i>P</i>	+

Three conformers for chromane **2** are found within the 3 kcal/mol energy window (Figure 7, Table 2). In the first two, **2a** and **2b**, populated in the conformational equilibrium at over 99%, the heterocyclic ring is in a half-chair conformation with the methyl ester substituent at C-2 in an axial and the methyl group in an equatorial position. The two conformers **2a** and **2b** differ in an arrangement of the carbonyl group of methyl ester relative to the aromatic ring. In the lowest energy **2a** conformer, the C=O group points away from the benzene ring, whereas it points toward this ring in the **2b** conformer. In the **2c** conformer, higher in energy by 2.7 kcal/mol and populated in the conformational equilibrium less than 1%, the heterocyclic ring adopts also a half-chair conformation. This time the methyl ester and methyl groups at C-2 accept an equatorial and an axial position, respectively (Figure 7).

However, the calculated sign of the 1L_b ECD band remains the same despite the change of helicity in the dihydropyran ring from *M* for **2a** and **2b** to *P* for **2c** (Table 2).

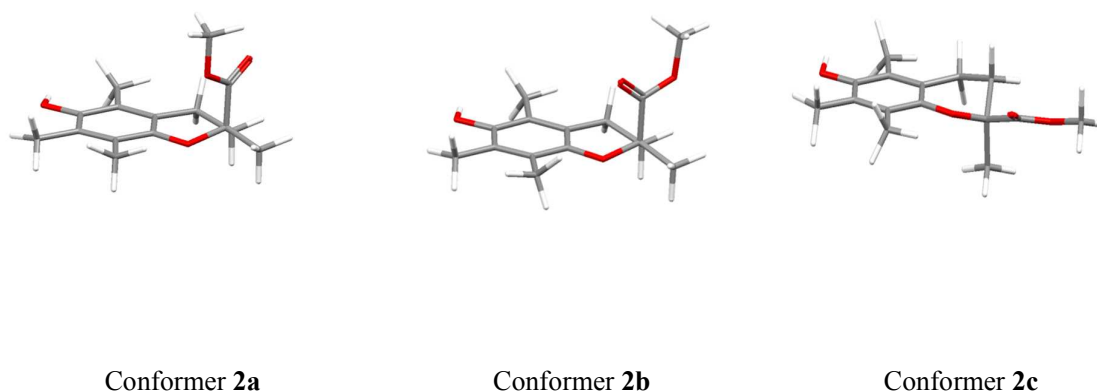


Figure 7. Optimized structures of chromane **2** conformers calculated at the B3LYP/6-31G(d) level of theory and projections of the dihydropyran ring viewed along the aromatic ring intersecting its position 6 and 7.

The structure of the lowest energy conformer **2a** is in a truly good agreement with the solid-state structure, considering data shown in Table 3 and comparison of structures in Figure 8.

Table 3. Selected torsional angles in degree ($^\circ$) determined by the X-ray diffraction for **2** and calculated for lowest energy conformer **2a** by B3LYP/6-31G(d) method. Atom numbering as in Figure 1.

	8a-O-2-3	O-2-3-4	2-3-4-4a	3-4-4a-8a	4-4a-8a-O	4a-8a-O-2	8a-O-2-C _{ester}
X-Ray 2A	-52.5	60.0	-36.7	7.2	-0.8	23.0	70.2
X-Ray 2B	-58.0	57.2	-31.2	6.7	-7.1	33.9	65.1
Conf. 2a	-49.8	59.3	-40.2	11.9	-0.8	21.1	72.6



Figure 8. Comparison of the X-ray structure of **2** (green) with the structure of the lowest energy conformer **2a** (blue) calculated at the B3LYP/6-31G(d) level of theory. Left: overlay of chromane **2** crystallographic and computed structures of molecule A, right: overlay of crystallographic and computed structures of molecule B.

A very good agreement between the solid-state and computed structures (Table 3), as well as the close similarity of the ECD spectra of **2** recorded in both solid-state and solution (Figure 9), suggests the crystal structure was close to the predominant structure seen in solution. This indicates that the solute-solvent interactions, which may considerably affect the ECD spectra owing to both conformational and vicinal effects, are negligible in this case. Therefore, the analysis of the ECD data can be performed on the basis of chiroptical data obtained for solutions. The minor differences seen in the ECD spectra in both states, such as *e.g.* a ~ 10 nm red-shift of bands in the solid state spectrum *versus* liquid state (Figure 9 left), can be accounted for considering the significant role played by the packing forces. Nevertheless, the positioning of the bands and their sign pattern are consistent in both states. Although, Pescitelli *et al.*⁴⁹ demonstrated recently that TDDFT calculations, which were based on the X-ray structure, reproduce very well the lattice effects on the ECD spectra, the application of this methodology went beyond the scope of this work.

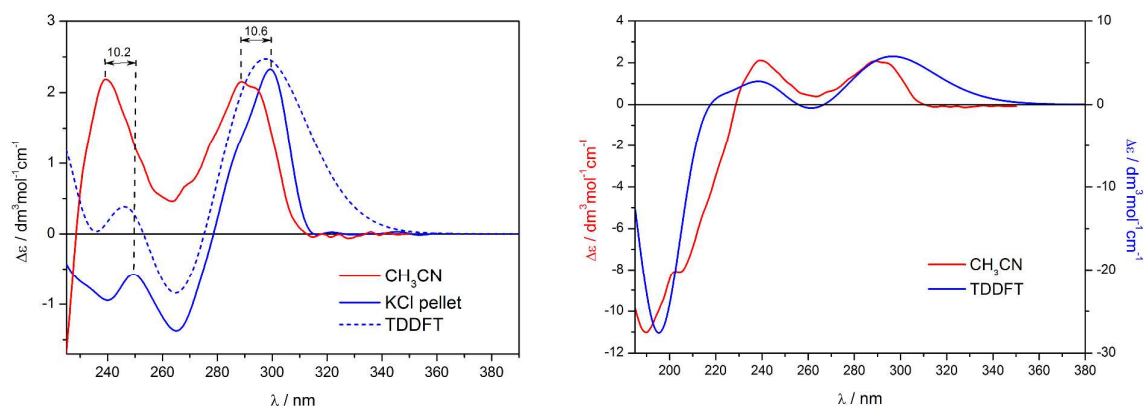


Figure 9. Left: ECD spectra of chromane **2** recorded in acetonitrile (solid red line) and in KCl pellet (solid blue line) both presented over the range 390-225 nm with ECD spectrum computed at the B3LYP/6-311++G(d,p) level of theory based on X-ray structure (dotted blue line, value of R_{vel} divided by 6); Right: Computed ECD spectrum at the B3LYP/6-311++G(d,p)/PCM(CH₃CN) level of theory obtained as a population-weighted sum at 298 K of individual conformers of **2** (blue line) compared to experiment in CH₃CN (red line). The symbol $\Delta\epsilon$ denotes the difference of the molar decadic absorption coefficients of left and right circularly polarized light ($\Delta\epsilon$ and $\Delta\epsilon$ denotes experimental and theoretical $\Delta\epsilon$, respectively), λ the wavelength, and R_{vel} the rotatory strength.

The Boltzmann-averaged ECD spectrum being by definition the sum of contributions from all conformers and weighted according to their population percentages shows the very satisfactory agreement between experiment and theory. Thus, the strong evidence that these conformers are present in a solution under these conditions is provided. As predicted by TDDFT calculations, the excitations at 291.5 nm and 271.5 nm can be reasonably attributed to the transition from HOMO to LUMO and HOMO to LUMO+1 of **2a**, likely corresponding to a substituted benzene ring $\pi\pi^*$ transitions (Figure 10). In addition, some contributions of the $n\pi^*$ transitions of the ester group at the C-2 carbon atom and from non-bonding orbitals of pyran oxygen free electron pairs are also visible.

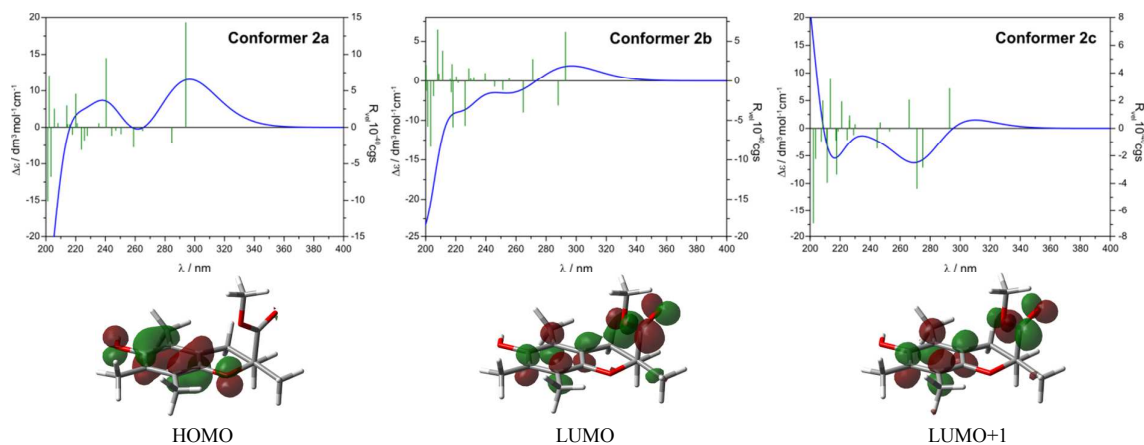


Figure 10. Top: Simulated ECD spectra of chromane **2** conformers at B3LYP/6-31++G(d,p)/PCM(CH₃CN) level of theory. The symbol R_{vel} denotes the computed rotatory strength; Bottom: MOs of individual excitations of chromane **2** lowest energy conformer with dominant contributions.

The results for **2** demonstrate a very good conformity between the calculated and the experimental values for both solid and solution states, thereby supporting the correctness of the computational procedure adopted. Thus, the same calculation methodology was applied for the remaining chromanes. The aim of these calculations is to check the necessity of verification of the chromane helicity rule results by theory. The comprehensive results of the conformational analysis and ECD spectra simulations for compounds **1**, **3-7** are given in the

Supporting Information (Figure S3–S14) while the selection of the most relevant ones is presented and discussed below.

Five conformers are found for trolox **1** within the energy range of 3 kcal/mol (Table 4). Two lowest energy structures, namely **1a** and **1b**, are populated in the conformational equilibrium at over 92%. Similarly, as for the (*S*)-trolox methyl ester (**2**), the heterocyclic ring in these two conformers adopts a half-chair conformation with the carboxyl substituent at C-2 in an axial position. The only difference in **1a** and **1b** is the arrangement of the carboxyl group relative to the aromatic ring. In the remaining three conformers with the *P* helicity of the dihydropyran ring, the carboxyl substituent occupies an equatorial position. These latter conformers (**1c–1e**) are computed to be at least 1.76 kcal/mol [B3LYP/6-31G(d)] higher in energy than the lowest energy conformer **1a**. Therefore, their population is negligible at room temperature. Also for this reason, there is apparently no difference between the simulated ECD spectrum of conformer **1a** and the Boltzmann-averaged spectrum (see the Supporting Information, Figure S3 and S4).

Only **3c** conformer of chromane **3** adopts *P* helicity in contrast to its lower energy conformational partners of *M* helicity (**3a** and **3b**). However, regardless of the ring helicity, the computed 1L_b band is positive in each case. As can be seen in Table 4, a very similar situation occurs in the other two cases, namely chromanes **4** and **5**. All five conformers of **4** and three of **5** adopts a half-chair geometry of the chromane ring. The most notable differences among these conformers are seen in the orientation of the largest substituent at C-2. Four and two of the conformers of **4** and **5**, respectively, including the most stable ones (populated *ca.* 45% and 49%, respectively), have this substituent in the axial position while in the remaining structures, it accepts the equatorial position. These results clearly show that the predictions made using the chromane helicity rule will not necessarily be correct.

An additional proof of the above statement came from the vibrational circular dichroism (VCD) spectroscopy. Nowadays, such a combined approach of more than one chiroptical method is widely recognized as necessary in order to arrive at the reliable configurational assignment.⁴⁰ As a model compound for the VCD study (*S*)-trolox methyl ester acetate (**4**) was chosen. This compound was selected because it does not form hydrogen bonds and, consequently, the interpretation of VCD results will be greatly facilitated. The VCD and IR spectra were recorded in CDCl₃, and the concentration was adjusted to the 1500–950 cm⁻¹ range. The spectra were calculated for the same population of conformers as for ECD spectra using B3LYP functional and various bases: 6-31G (d), 6-311++G(d,p) and TZVP. The best fit of the experimental and theoretical spectra was obtained for the TZVP basis (Figure 11). For this base (TZVP) the similarity coefficient calculated using the algorithm CompareVOA⁵⁰ was 85.3% for (*S*) enantiomer and the enantiomeric similarity coefficient (ESI) was equal to 79.5% with a confidence level of 100%. The experimental and calculated IR and VCD spectra compare pretty well: the sign and the absolute intensities of most VCD signals are well reproduced.

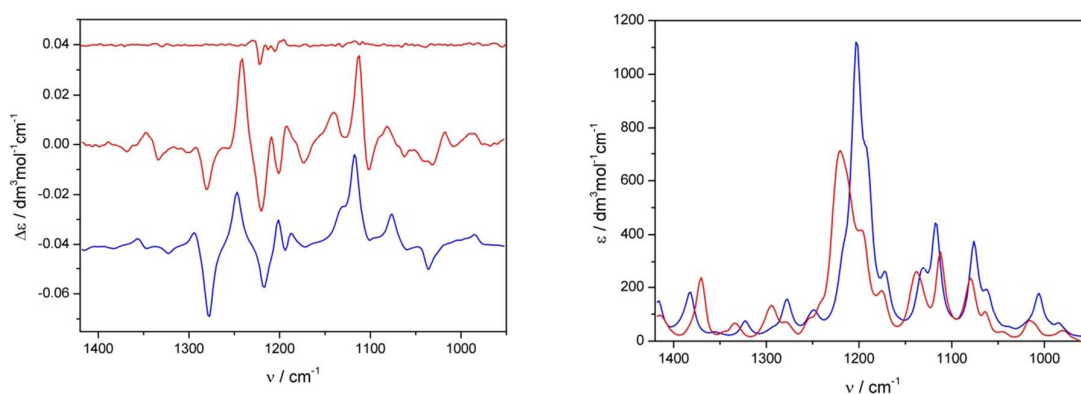


Figure 11. Experimental (red) and simulated at B3LYP/TZVP level of theory (blue) VCD (left) spectra obtained as a population-weighted sum at 298 K of individual conformers with noise level and IR spectra (right) of (*S*)-trolox methyl ester acetate (**4**). Spectra measured in CDCl₃.

The overall agreement of the predicted and experimental VCD spectra independently supports the configurational and conformational assignment of **4** obtained from the ECD

studies. Therefore, one can say that such a combined use of different chiroptical methods for three-dimensional structure determination allows for an unambiguous stereochemical assignment as it provides an independent verification of the results.

Only two conformers are found for chromane **6** in the 5 kcal/mol energy window. However, the lowest energy conformer of *M* helicity and its population of nearly one hundred percent is of key importance for the ECD spectra. The contribution of the next conformer, higher in energy by more than 4 kcal/mol, is negligible at room temperature. Very similar situation is found for the acetyl derivative of **6**, namely chromane **7**. Although four conformers are found for **7** in the 5 kcal/mol energy range, only the first two contribute significantly to the net ECD spectrum. Conformers **7c** and **7d**, because of a very low population and a high energy, could be eliminated from further considerations. It should be noted that regardless of *M* or *P* helicity, calculations predict the same sign of the long-wavelength ECD band for all conformers **7a-7d** (Table 4).

Table 4. Overview of the conformer (conf.) analysis for chromanes **1** and **3-7**: Gibbs free energy (ΔG) calculated at the B3LYP/6-31G(d) level of theory in kcal/mol, population (pop) at 298 K in %, C8a–O–C2–C3 torsion angle in degree ($^\circ$) and calculated sign of the ECD of the 1L_b ECD band. Atom numbering as in Figure 1.

Comp.	Conf.	ΔG	Pop.	C8a–O–C2–C3	Helicity	Sign of 1L_b band
1	1a	0.00	76.6	–49.2	<i>M</i>	+
	1b	0.94	15.5	–47.2	<i>M</i>	+
	1c	1.76	3.9	+48.5	<i>P</i>	–
	1d	1.93	2.9	+44.3	<i>P</i>	–
	1e	2.56	1.0	+47.6	<i>P</i>	+
3	3a	0.00	57.5	–44.5	<i>M</i>	+
	3b	0.21	40.0	–45.1	<i>M</i>	+
	3c	1.90	2.3	+46.8	<i>P</i>	+
4	4a	0.00	44.8	–45.6	<i>M</i>	+
	4b	0.36	24.4	–48.1	<i>M</i>	+
	4c	0.46	20.5	–43.9	<i>M</i>	+
	4d	1.14	6.6	–45.3	<i>M</i>	+
	4e	1.48	3.7	+43.2	<i>P</i>	+
5	5a	0.00	49.2	–39.4	<i>M</i>	+
	5b	0.34	35.0	–38.5	<i>M</i>	+

	5c	1.13	15.8	+47.0	<i>P</i>	-/+
6	6a	0.00	98.8	-47.3	<i>M</i>	+
	6b	4.38	2.2	+48.6	<i>P</i>	-
7	7a	0.00	78.87	-45.4	<i>M</i>	+
	7b	1.51	17.35	-45.6	<i>M</i>	+
	7c	3.35	2.76	+45.7	<i>P</i>	+
	7d	4.35	1.02	+47.6	<i>P</i>	+

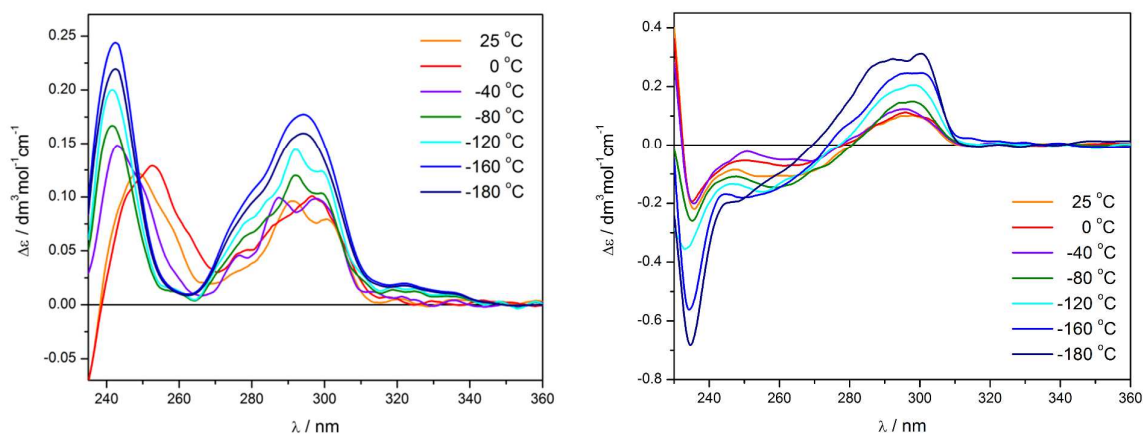
The second group of compounds (chromanes **8-11**) is characterized by a much lower intensity of ECD bands across the whole spectrum. As expected, the conformational composition of chromanes **8-11** is much more complex what is manifested by a small energy difference between conformers. For example, conformational analysis of chromane **8**, performed within the 5 kcal/mol energy window, found four conformers differing only very slightly in energy (Table 5).

Table 5. Overview of the conformer (conf.) analysis for chromanes **8-11**: Gibbs free energy (ΔG) calculated at B3LYP/TZVP level, population (pop) at 298 K in %, C8a-O-C2-C3 torsion angle in degree ($^\circ$) and signs of the 1L_b ECD band calculated at B3LYP/6-311++G(d,p)^(a) and B3LYP/TZVP^(b) levels of theory.* Atom numbering as in Figure 1, and +/- or -/+ in the last column indicate a bisignate ECD band of a given signs sequence.

	Conf.	ΔG	Pop.	C8a-O-C2-C3	Helicity	Sign of 1L_b band
8	8a	0.00	28.5	-46.4	<i>M</i>	+ ^(b)
	8b	0.10	26.0	+46.6	<i>P</i>	- ^(b)
	8c	0.18	24.0	-46.5	<i>M</i>	+ ^(b)
	8d	0.33	21.5	+46.7	<i>P</i>	- ^(b)
9	9a	0.00	38.6	-40.83	<i>M</i>	- ^(b)
	9b	0.20	27.5	-41.20	<i>M</i>	- ^(b)
	9c	0.87	8.9	-49.13	<i>M</i>	+/- ^(b)
	9d	0.94	7.9	+47.07	<i>P</i>	-/+ ^(b)
	9e	1.01	7.0	+47.00	<i>P</i>	-/+ ^(b)
	9f	1.10	6.0	-49.44	<i>M</i>	+/- ^(b)
	9g	1.68	2.2	+46.75	<i>P</i>	-/+ ^(b)
	9h	1.78	1.9	+47.11	<i>P</i>	-/+ ^(b)
10	10a	0.00	53.5	-46.4	<i>M</i>	- ^(a)
	10b	0.14	46.5	+47.2	<i>P</i>	+ ^(a)
	10a	0.00	57.1	+47.2	<i>P</i>	- ^(b)
	10b	0.29	42.9	-46.4	<i>M</i>	+ ^(b)
11	11a	0.00	64.0	-41.8	<i>M</i>	+ ^(a)
	11b	0.57	36.0	+47.4	<i>P</i>	+ ^(a)
	11a	0.00	68.0	-41.8	<i>M</i>	+ ^(b)
	11b	0.77	32.0	+47.4	<i>P</i>	- ^(b)

* Explanation regarding the use of different levels of theory is to be found in the text.

It appears that the conformational space of chromane **8** contains roughly an equal amount of *M* and *P* conformers with only a small predominance (2.5%) of the *M* helical conformers (see the Supporting Information, Figure S15 and S16). Therefore, in the ECD spectrum recorded at room temperature as being the sum of all contributing conformers, a positive 1L_b band of low intensity reflects a small preponderance of *M* conformers. As shown in Figure 12, lowering the temperature of measurements results only in a slight increase in the intensity of these bands in both polar (EPA: Et₂O/isopentane/EtOH, 5:5:2, v/v) and non-polar solvents (MI₁₃: methylcyclohexane/isopentane, 1:3, v/v). That additionally validates a slight dominance of conformers *M* over *P* in the equilibrium. In turn, this increase of intensity of the ECD bands at a lower temperature results on account of the greater conformational homogeneity favoring the most stable conformer. Noteworthy is the influence of the solvent on the other ECD bands of **8** manifested even in their sign change, e.g. 1L_a band at ~240 nm from Figure 12. A blue-shift of some maxima observed at low temperatures can be attributed to the solute-solvent interaction.



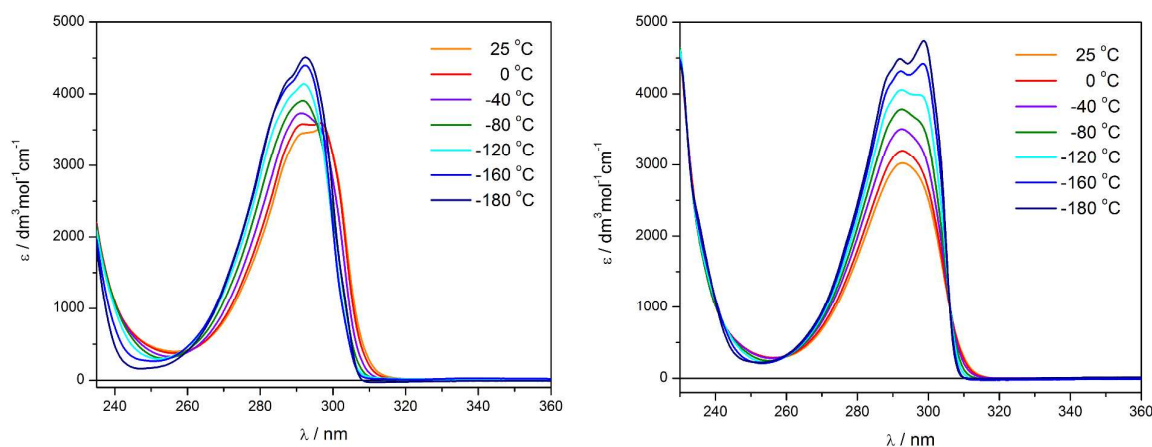


Figure 12. ECD (top) and UV-Vis (bottom) spectra of chromane **8** recorded in EPA (right) and MI₁₃ (left). The symbol ϵ denotes the molar decadic absorption coefficient, $\Delta\epsilon$ – the difference of the molar decadic absorption coefficients of left and right circularly polarized light, and λ – the wavelength.

To determine contributing conformers of chromane **9**, conformational analysis was performed with MM+ force field. Next, structures of all conformers found were re-optimized at B3LYP/TZVP level of theory, including PCM model for acetonitrile. As a result, eight conformers were found within 3 kcal/mol energy range (Table 5). In the next step the ECD spectra of each conformer found (conformers **9a** to **9h**) were simulated with the B3LYP functional and TZVP basis set, using the PCM solvent continuum model with acetonitrile as a solvent. The predicted ECD spectrum, weighted on the basis of the Gibbs free energy, is shown in Figure 13. As can be seen, the Boltzmann averaged ECD spectrum of compound **9** is in a very good agreement with the experimental spectrum.

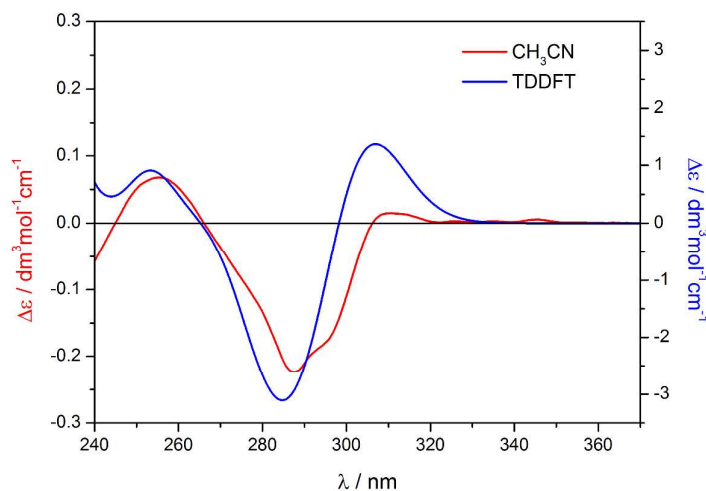


Figure 13. Comparison of experimental ECD spectrum of chromane **9** with its Boltzmann averaged simulated spectrum at B3LYP/TZVP/PCM(CH₃CN) level of theory.

The geometry of the three lowest energy conformers of **9**, namely conformers **9a**, **9c**, and **9d**, together with their simulated ECD spectra is shown in Figure 14 (the geometry and simulated ECD spectra of the remaining conformers as well as the MOs involved are deposited in the Supporting Information, Figure S17). The diagnostic ¹L_b band in the corresponding spectra is negative or bisignate. This difference is due to the different orientation of the vinyl substituent relative to the chromane ring. In the case of **9a**, the vinyl group is directed to the inside of the molecule whereas in the case of the **9c** outside. For conformer **9d** this band is also bisignate, but with opposite sign sequence than **9c**. The positive band above 300 nm comes from the excitation of the vinyl double bond which mixes with chromane transitions. These vinyl transitions are particularly visible in the ECD spectra of conformers **9c** and **9f** constituting 10% of the equilibrium mixture (Figure 14). However, in the UV spectrum the olefinic band is hidden under aromatic absorption.

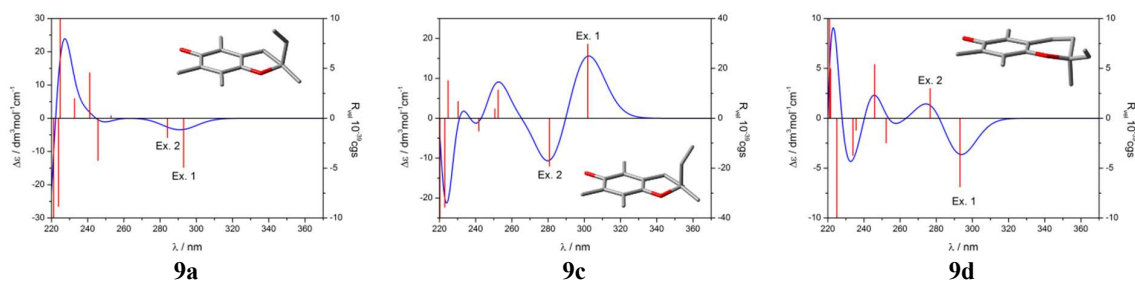


Figure 14. Simulated ECD spectra and structures of the three lowest energy conformers of compound **9** calculated at the B3LYP/TZVP/PCM(CH₃CN) level of theory (conformer **9b** was omitted because of only a slight difference in the torsion angle value equal to 0.37 ° compared to conformer **9a**).

In the context of the chromane helicity rule, the lowest energy conformer **9a** does not comply with the rule because it exhibits CEs of opposite signs to those required by the rule. It generates a negative CE in the range of ¹L_b band instead of a positive predicted by the rule for the *M* helicity. On the other hand, the Boltzmann-averaged ECD spectrum shows the very

satisfactory agreement between experiment and theory (Figure 13). This corroborates the existence in the equilibrium of all calculated conformers presented in Table 5.

The further extension of the side-chain length at C-2 in chromanes may enhance their relatively unrestricted mobility, limited to the great extent to the side chain substituent only. As a consequence, a sign change could occur as different conformers can make different contributions to the total ensemble-averaged spectrum. Specifically, this is reflected in the compounds **10** and **11**, in which a sign change of the decisive CE at ~290 nm takes place without a change of the stereochemical arrangement at the stereogenic center, compared to chromane **8** (Table 1). The negative sign of this CE in the experimental spectra of **10** and **11** is consistent with the chromane helicity rule as appropriate for *P* conformer with equatorially oriented C₆H₁₃ and C₆H₁₁ substituents, respectively. This was to be expected because the percent of the equatorial conformation should increase with increasing steric interaction of prolonged alkyl substituent at C-2.⁵¹

A validation of this statement by calculation is not a trivial task. With increasing length of the alkyl substituent on carbon C-2 the conformational lability of the side chain increases, too. Therefore, the conformational analysis of such systems, conducted to find contributing conformers, is significantly impeded. To reduce both time and the cost of calculations, the conformational analysis of chromanes **10** and **11** was carried out for *M* and *P* conformers of tetrahydropyran ring with a frozen conformation of the side chain at C-2. This frozen conformation was adapted from the single crystal X-ray conformation of an analog of α -tocopherol.⁵² The conformers were obtained by a substitution of the phytyl chain by a shorter, six-carbon long analogs and subsequent optimization of obtained structures. The geometry optimizations and thermochemistry calculations were conducted at B3LYP/6-311++G(d,p)/PCM(CH₃CN) and B3LYP/TZVP/PCM(CH₃CN) levels of theory.

In calculations of chromane **10** at B3LYP/6-311++G(d,p)/PCM(CH₃CN) level of theory, conformer *P* with an equatorially oriented bulky substituent but a positive CE at ~290 nm was predominant (Figure 15). This contradicted the chromane helicity rule, which for the *P* conformers predicts negative CEs in this spectral region. On the other hand, calculations carried out at B3LYP/TZVP/PCM(CH₃CN) level of theory predicted for the lowest energy *P* conformer a negative sign of the same ECD band (Figure 15). Thus, the simulated spectra show a strong dependence on the applied basis set. Such a dependence of TDDFT calculation on the tentative functionals and basis sets used is well known in the literature.^{53, 54} However, preliminary results for chromans **9** and **10** obtained with the functional involving a correction for long range correlation effects, namely CAM-B3LYP and TZVP basis set are consistent with the results from the B3LYP functional and the same basis set (see Figure S19 in Supporting Information).

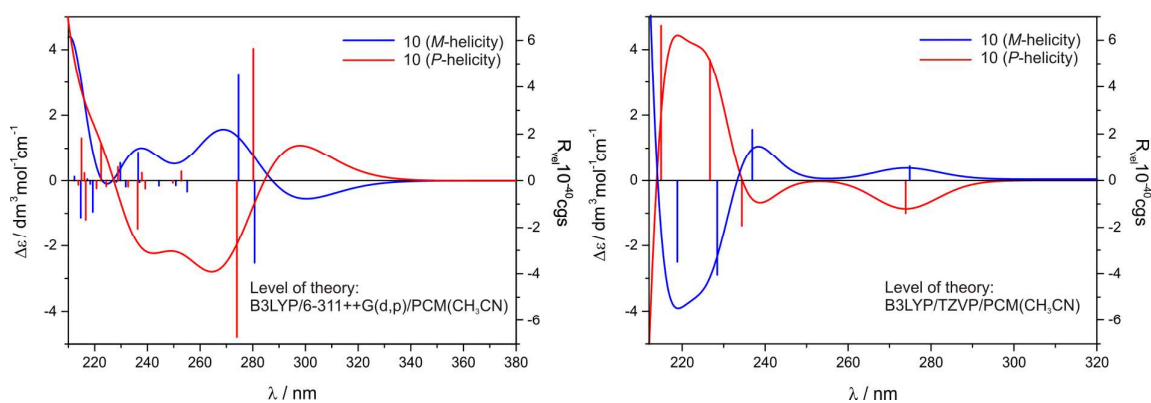


Figure 15. Simulated ECD spectra of *M*- and *P*-conformers of chromane **10** calculated at B3LYP/6-311++G(d,p)/PCM(CH₃CN) and B3LYP/TZVP/PCM(CH₃CN) levels of theory left and right, respectively.

In the case of **10**, the ECD spectra of conformers **10a** and **10b** differing by 0.14 or 0.29 kcal/mol depending on the basis set used, are almost mirror images clearly indicating the different conformations of the heterocyclic ring. According to the calculations, the excitations within the long wavelength ECD band can be reasonably attributed to the transitions from HOMO to LUMO and HOMO to LUMO+1 in both *M* and *P* conformers of **10**, likely

corresponding to a substituted benzene ring $\pi\pi^*$ transitions. Besides, these transitions are not pure and involve also non-binding orbitals of pyran oxygen free electron pairs (Figure 16).

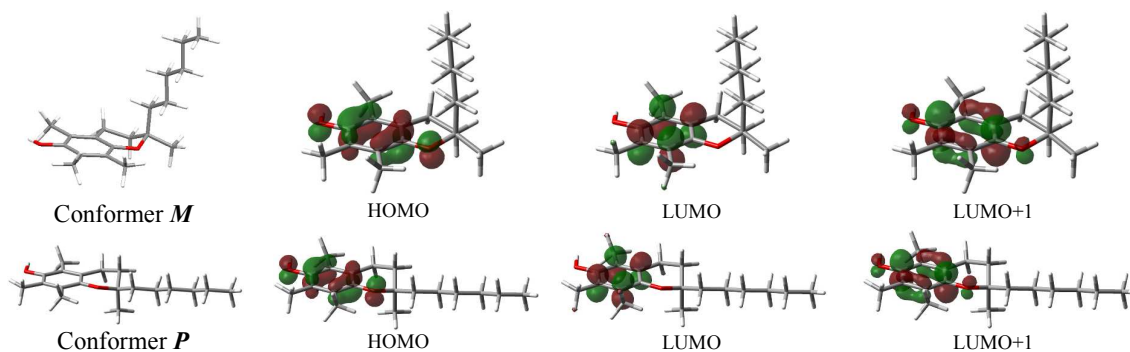


Figure 16. Structures of *M* and *P* conformers and MOs of individual excitations of two conformers with dominant contributions of chromane **10**.

Since the reliability of theoretical predictions greatly facilitates comparison with experimental data or results obtained from complementary methods, we attempted variable temperature ECD measurements of **10** to enhance the results of calculations. Measurements made in both polar (EPA) and non-polar (MI₁₃) solvents clearly show conformational instability of chromane **10**. In both solvents, already below -80 °C the ECD curve become bisignate which clearly indicates the presence of roughly equal amounts of *M* and *P* conformers in equilibrium (Figure 17). Additional decrease of the temperature shifts the equilibrium toward the conformer characterizing by a positive CE. Thus, simultaneously with decreasing temperature the positive band become much more pronounced at the expense of the negative one, which finally completely disappears.

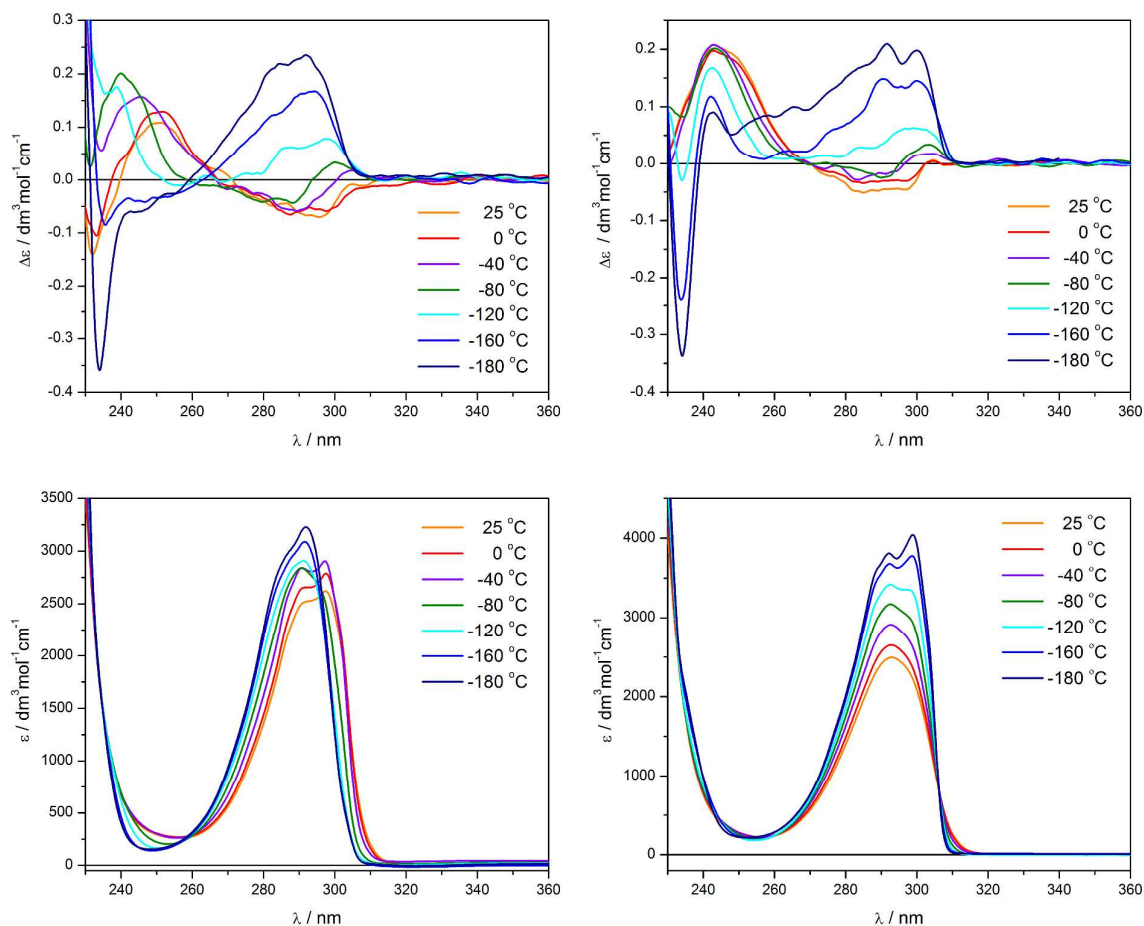


Figure 17. ECD spectra of chromane **10** recorded in EPA (right) and MI₁₃ (left). The symbol ε denotes the molar decadic absorption coefficient, $\Delta\varepsilon$ – the difference of the molar decadic absorption coefficients of left and right circularly polarized light, and λ – the wavelength.

The chromane **11** with the unsaturated C₆H₁₁ side chain demonstrates very similar behaviour. Two negative weak CEs in its experimental spectrum occurring at 289.0 and 296.0 nm are associated with the ¹L_b chromane excitation. Furthermore, there is also a very weak positive CE at 308.5 nm. This band is associated with transitions from HOMO to LUMO orbitals of the chromane ring with substantial contributions of olefinic electrons of the unsaturated substituent at C-2. Similarly as in the case of chromane **9**, in the UV spectrum of **11** the olefinic absorption bands are not visible as they are hidden under aromatic absorption.

Simplified conformational analysis was conducted analogously as for chromane **10**, *i.e.* with a frozen side chain substituent. Contrary to the prior case and regardless of the basis

set used, the values of free energy differences in chromane **11** show a full predominance of the *M* conformer with an axial C₆H₁₁ substituent at C-2 over the *P* conformer (Table 5). ECD spectra of generated *M* and *P* conformers, computed at B3LYP/6-311++G(d,p)/PCM(CH₃CN) level of theory, show opposite signs of transitions within ¹L_b band, positive and negative respectively (Figure 18). Both applied basis sets agreeably predict for the *M* conformer a positive sign of the main band, thus incorrectly reproducing experimental data. Furthermore, the equilibrium preference for conformer with a long alkenyl substituent on C-2 carbon in an axial position is contradictory to the previous literature reports.⁵¹ Also in this case the use of CAM-B3LYP functional in place of B3LYP resulted in no observable changes in the calculated spectrum.

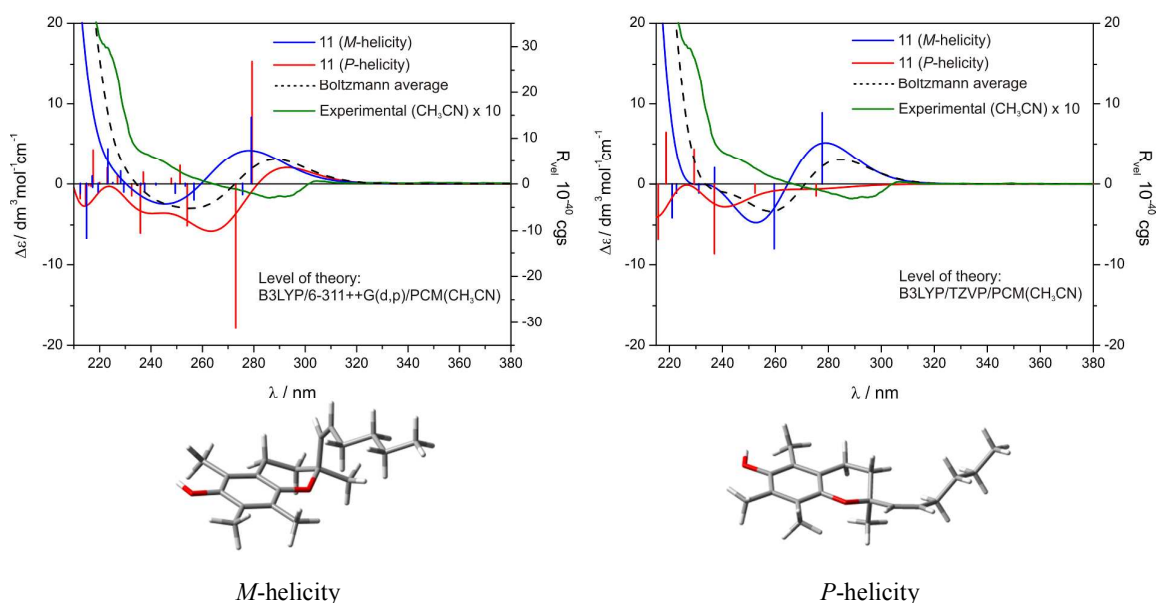


Figure 18. Comparison of experimental ECD spectrum of **11** with simulated spectra of its *M* and *P* conformers together with Boltzmann average curve and optimized at B3LYP/6-311++G(d,p)/PCM(CH₃CN) and B3LYP/TZVP/PCM(CH₃CN) levels of theory structures of *M* (left) and *P* conformers (right). R_{vel} values are diminished fourfold.

Next, to get more insight into incompatibility between theory and experiment we analyzed the electric (μ_e) and the magnetic (μ_m) transition dipole moment values and the relative angle between them (see Table S1 in Supporting Information). It is surely well known that the angle θ between these two moments and their magnitudes independently contribute to

the observed CEs. It turns out that the good compliance of theory with experiment is reached when the angle θ considerably deviates from 90° . For values θ close to 90° , like in some conformers of compounds **8**, **10**, and **11**, there is no clear correlation.

Given the inconsistencies in the calculation results for chromane **11**, we decided to support the theoretical results by the variable temperatures measurements. In this case, a sign change of the long-wavelength 1L_b band resulting from a decrease of temperature occurred only in the non-polar solvent MI_{13} (Figure 19). This appears to be a case of a strong influence of the solvent, which likely manifests itself in either stabilization or destabilization of investigated structures.

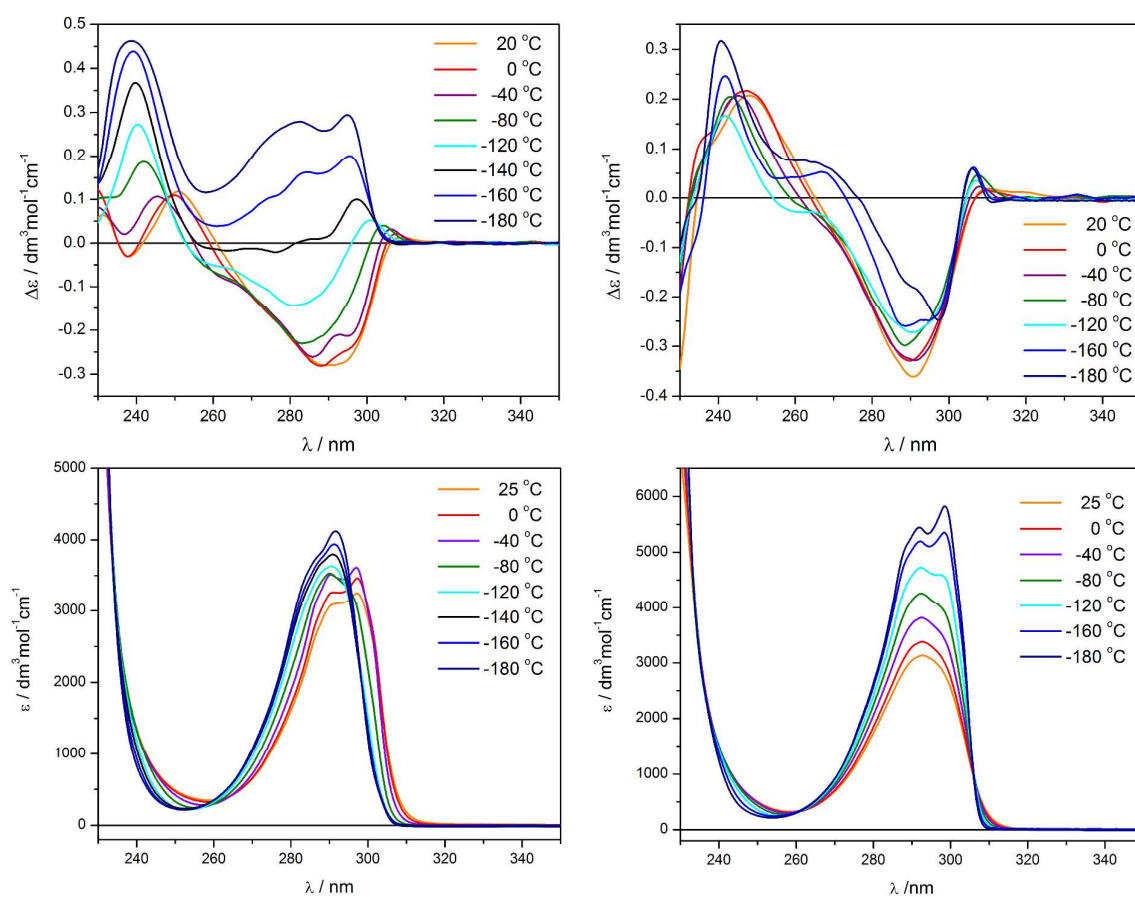


Figure 19. ECD spectra of chromane **11** recorded in EPA (right) and MI_{13} (left) at various temperatures. The symbol ϵ denotes the molar decadic absorption coefficient, $\Delta\epsilon$ – the difference of the molar decadic absorption coefficients of left and right circularly polarized light, and λ – the wavelength.

The results of ECD measurement within a relatively large temperature range may also be a source of a quite accurate information on the distribution of conformers in flexible, optically active molecules.^{48, 53, 55} Therefore, we used the method developed for this purpose by Moscovitz *et al.*⁴⁸ This method allows the verification of relative energy of the conformers obtained from calculations and the estimation of the experimental conformer distribution for chromans **10** and **11**. By definition, it can only be applied to a mixture of two conformers. As a result, a plot of rotational strength R^T against $1/[1+\exp(-\Delta G^0/RT)]$ provides a family of curves of which only the straight line corresponds to the right and, therefore, experimental ΔG^0 (components of the equation from above are explained in the caption to Figure 20). Subsequently, as a result of graphical operation, the experimental values of conformer distribution and rotational strength of isolated components can be obtained.

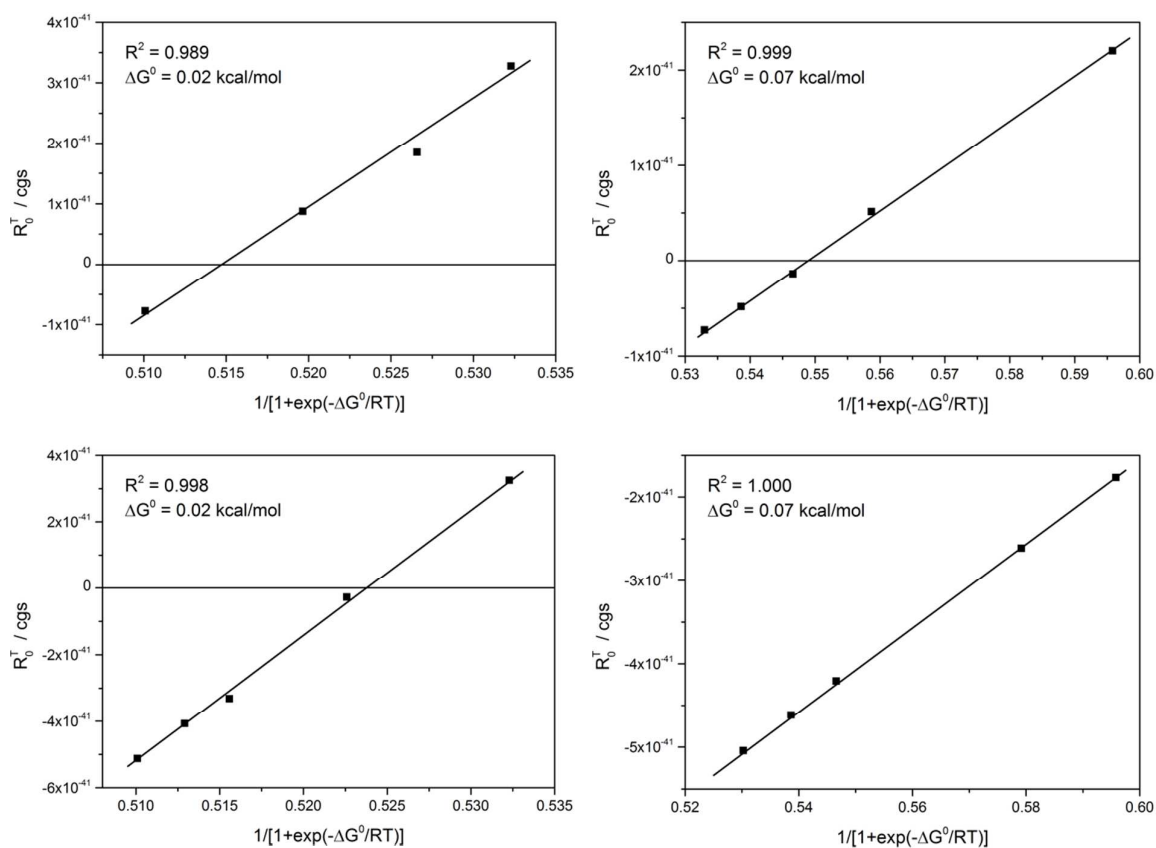


Figure 20. Plot of R_0^T against $1/[1+\exp(-\Delta G^0/RT)]$ of **10** (top) and **11** (bottom) in MI_{13} (left) and EPA (right). R_0^T denotes observed total rotational strength at selected temperature T (K); R on the x-axis is the gas constant, R^2 denotes coefficient of determination and ΔG^0 is the

standard Gibbs free energy for the conformational change between *P*- and *M*-helicity of chromane ring.

Detailed results obtained with the method of Moskowitz for chromans **10** and **11** are summarized in Table 7 and Figure 20. Similarly to the calculations results, the ΔG^0 values obtained for both MI₁₃ and EPA solvents show that the difference in relative energy between *P* and *M* conformers is very small. In the case of **10**, this manifests itself clearly in the sign change of the ¹L_b band in both solvents used whereas in the case of **11** the sign change occurs in MI₁₃ only.

Table 7. Calculated values for the rotational strengths R_a and R_b of chromans **10** and **11** in polar (EPA: ethanol-isopentane-diethyl ether, 2:5:5, v/v) and non-polar (MI₁₃: methylcyclohexane-isopentane, 1:3, v/v) solvents as well distribution of conformers in various temperatures. R_a denotes the rotational strengths of lower energy conformer "a" and R_b the higher energy conformer "b", X_a denotes the molar fraction of lower energy conformer and X_b the higher energy conformer.*

T/°C	R_a /cgs	R_b /cgs	Chromane 10				Chromane 11			
	Chromane 10		X_a		X_b		X_a		X_b	
	MI ₁₃		MI ₁₃	EPA	MI ₁₃	EPA	MI ₁₃	EPA	MI ₁₃	EPA
25	8.59x10 ⁻⁴⁰	-9.11x10 ⁻⁴⁰	0.51	0.54	0.49	0.46	0.51	0.53	0.49	0.47
0	EPA		0.51	0.54	0.49	0.46	0.51	0.54	0.49	0.46
-40	2.10x10 ⁻⁴⁰	-2.60x10 ⁻⁴⁰	0.51	0.54	0.49	0.46	0.52	0.54	0.48	0.46
-80	Chromane 11		0.51	0.55	0.49	0.45	0.52	0.56	0.48	0.44
-120	MI ₁₃		0.52	0.57	0.48	0.43	0.52	0.57	0.48	0.43
-140	18.0x10 ⁻⁴⁰	-20.0x10 ⁻⁴⁰					0.53		0.47	
-160	EPA		0.53	0.60	0.47	0.40	0.53	0.58	0.47	0.42
-180	1.8x10 ⁻⁴⁰	-3.1x10 ⁻⁴⁰	0.53	0.60	0.47	0.40	0.54	0.60	0.46	0.40

*The accuracy of molar fractions of particular conformers is far less than the number of decimal places given in the Table. This accuracy, however, is maintained to show the relative trend of the conformational composition.

Uncertainty regarding the structure of conformers, primarily in the case of chromanes **10** and **11**, can be related to the simplification adopted in the conformational analysis eliminating a number of possible rotamers. Another significant reason for this can be a lack of consideration of solvent effects during the geometry optimization. As recently reported, the introduction of solvent effect at the both stages of computation, namely geometry optimization and simulation of the ECD spectra, may substantially increase accuracy of the subsequent TDDFT/B3LYP results for the total rotatory power.⁵⁶ An investigation of

chromanes with a long side chain at C-2 clearly identifies the problems arising during the determination of the stereostructure of floppy systems on the basis of a limited number of conformers. Because of a high degree of conformational flexibility these compounds pose a challenge, primarily in terms of computation complexity.

Despite discussed above problems, the results obtained for the flexible chromanes **8-11** are a foundation leading to some interesting insights. Extending the length of the alkyl side chain by a relatively small number of carbon atoms does not significantly affect the ECD spectrum.^{23,57} As can be seen on Figure 21 right, the UV-Vis absorption of all the compounds including α -tocopherol (**i**) with phytyl side chain at C-2 are nearly identical. However, the intensity of the ECD band at ~ 290 nm in α -tocopherol (**i**) is the same as in chromane **10** bearing a six-carbons alkyl chain only (Figure 21 left). Chromane **8** with shorter alkyl side chain than chromane **10** exhibits an opposite sign of this band. In turn, the intensity of the same band in chromane **11** with an unsaturated, and thereby less labile side chain, among other differences, is greater in comparison with α -tocopherol (**i**) and its saturated counterpart **10**. Moreover, the shape of the ECD spectrum of chromane **9** with a vinyl substituent on carbon C-2 is almost identical with its hexenyl analog **11**. This was to be expected for compounds having the same chromophoric unit. The slight difference in the intensity of the bands results from lower mobility of vinyl substituent compared to hexenyl.

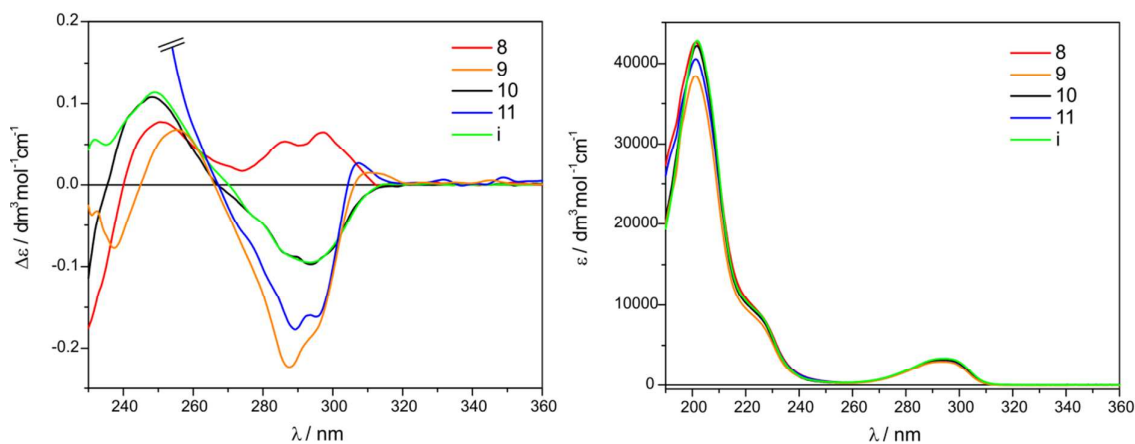


Figure 21. Comparison of UV-Vis (right) and ECD (left) spectra of chromanes **8-11** and α -tocopherol (**i**) recorded in acetonitrile. The symbol ϵ denotes the molar decadic absorption coefficient, $\Delta\epsilon$ – the difference of the molar decadic absorption coefficients of left and right circularly polarized light, and λ – the wavelength.

CONCLUSIONS

The main objective of this study was to test the range of applicability and reliability of chromane helicity rule. This rule was developed to assist with the assignment of absolute configuration of chromans. The rule, however, was found failing in regard to conformationally flexible compounds, such as certain chromans. In this work, a systematic analysis of a set of molecules with varied conformational flexibility was performed to check whether the general rule could be improved by offering some kind of refinement or modification. To this end, the relationship between the molecular structure and the chiroptical properties of trolox derivatives **1-11** was investigated by a single crystal X-ray diffraction analysis, electronic circular dichroism spectroscopy, especially with the variable low-temperature ECD measurements, vibrational circular dichroism, and TDDFT calculations.

As a result of these studies it was shown that in all investigated cases the conformation of chromane skeleton with a methyl substituent on C-2 carbon atom in an equatorial position predominates. The presence of the same conformation both in a solid phase and in a solution is experimentally confirmed by the ECD spectra recorded in both states. Moreover, calculations show a very good agreement between the lowest energy conformer structure and the solid-state structure.

The most important inference from the calculations is that in most cases the simulated ECD spectra of the conformers found for **1-11** do not conform to the chromane helicity rule, regardless of the *M*- or *P*-helicity of the dihydropyran ring. The results obtained for compounds with the known absolute configuration indicate that the ECD sign of the 1L_b band appears to be determined by two independent factors. The first factor is a twist of the

heterocyclic ring fused with the practically flat aromatic ring, while the second factor originates from disorders caused by the substituent/ents at the asymmetric carbon atom C-2. Depending on which of these two factors dominates, the 1L_b band shows a positive or negative CD. It may, therefore, happen that compound with the *P* (or *M*) configuration of the dihydropyran ring exhibits a positive or negative CD in the long-wavelength spectral range and *vice versa*. Most likely the object of our studies represents a system where its CD - using the classical nomenclature - is determined by a combination of a sector and a helicity rules.

The results presented herein clearly demonstrate that chromane helicity rule should always be applied cautiously, and the experimental data should be augmented with adequate quantum mechanical computational predictions in order to assign the absolute configuration with a high degree of confidence. It should also be emphasized that the use of more than one chiroptical technique will lead to a more reliable result. It should be noted, however, that in the present case ECD alone allows to solve the stereochemical problem without any ambiguity or doubt.

Summarizing, it turned out that the ECD spectroscopy is suitable for the comprehensive structural studies of chromans, as it is very sensitive to a minute changes in geometry and electronic structure of the investigated compounds. In this paper, we have demonstrated that the ECD measurements at variable temperatures are extremely useful for studies of both conformational homogeneity and complexity. The resulting conclusions, additionally supported by the calculations, offer a reliable support for the structural assignment.

It has to be added that the combination of experimental and theoretical results allows articulating a high quality conclusion about the relationship between the chiroptical properties and the detailed molecular structure of chromans. Recent progress in both equipment and computational methods leads to a much wider possibility of using chiroptical spectroscopy in

solving increasingly complex structural problems. Thus, the main conclusion of this paper is that semiempirical rules correlating the sign of an ECD band are no longer safe in assignment of absolute configuration. Since modern computational tools are nowadays readily available for routinely use even for non-specialists, a combined experimental and theoretical approach in solving stereochemical problems is strongly recommended.

EXPERIMENTAL SECTION

Source and synthesis of investigated compounds 1-11: Both enantiomeric Trolox derivatives (**1**, *ent-1*) i.e. (*S*)- and (*R*)-6-hydroxy-2,5,7,8-tetramethylchroman-2-carboxylic acid were purchased from Aldrich. The syntheses of compounds **2**,⁵⁸ **3**,⁴² **4**,⁵⁹ (M.p. 104-105 °C) **5**,⁴³ **6**,⁶⁰ **7**,⁶⁰ **8**,⁶¹ **9**,⁶² **10**,⁶³ (M.p. 49-50 °C) were carried out according to the literature methods. Compound **11** was prepared according to the procedure described in the Supporting Information together with its spectroscopic characterization.

General Information. All moisture-sensitive reactions were performed under argon atmosphere using oven-dried glassware. Anhydrous methanol was distilled from magnesium. Anhydrous THF was freshly distilled from sodium and benzophenone. Anhydrous DMF, DMSO, ethyl acetate (AcOEt) and dichloromethane (DCM) were distilled from CaH₂. Flash chromatography (FC) was carried out on Merck silica gel (230–400 mesh). Routine monitoring of reactions was performed using 60 F₂₅₄ silica gel TLC plates (Merck). TLC spots were visualized by heating plates sprayed with ammonium molybdate/cerium(IV) sulfate solution. Melting points were determined on a Mettler Toledo MP90. The ¹H and ¹³C NMR spectra were recorded on a Bruker Advance spectrometer (400 and 100 MHz, respectively) as solutions in CDCl₃. Chemical shifts are expressed in parts per million (ppm, δ) downfield from tetramethylsilane (TMS) and are referenced to CHCl₃ (77.4 ppm) as internal standard. Mass spectra were obtained at 70 eV with AMD-604 spectrometer. IR

spectra were recorded on a Nicolet series II Magna-IR 550 or Nicolet 6700 FT-IR spectrometer.

Single-Crystal X-ray Diffraction Studies. The X-ray measurement of **2** was performed at 100 (2) K on a diffractometer with graphite-monochromated Mo K α radiation (0.71073 Å). The crystal was positioned at 50.0 mm from the KM4CCD camera; 632 frames were measured at 1.0 ° on a counting time of 45s. Data reduction and analysis were carried out with the Oxford Diffraction programs.⁶⁴ The data were corrected for Lorentz and polarization effects and multi-scan absorption correction⁶⁵ was applied. The structure was solved by direct methods⁶⁶ and refined by using SHELXL.⁶⁷ The refinement was based on F² for all reflections except for those with very negative F². The weighted R factor, wR and all goodness-of-fit S values are based on F². The non-hydrogen atoms were refined anisotropically. The hydrogen atoms (except at hydroxyl group) were placed in calculated positions and refined within the riding model. The temperature factors of hydrogen atoms were not refined and were set to be equal to either 1.2 or 1.5 times larger than U_{eq} of the corresponding heavy atom. The hydrogen atoms at hydroxyl groups were found from a map and refined isotropically. The atomic scattering factors were taken from the International Tables.⁶⁸

ECD measurements. The electronic circular dichroism (ECD) spectra were recorded between 450–180 nm at room temperature in spectroscopic grade acetonitrile. Solutions of **1-11** with concentrations in the range from 4.0×10^{-4} to 8.5×10^{-4} M were examined in quartz cell with path length of 2–0.05 cm. All spectra were recorded using 100 nm/min scanning speed, a step size of 0.2 nm, a bandwidth of 1 nm, a response time of 0.5 sec, and an accumulation of 5 scans. The spectra were background corrected.

Low-temperature ECD measurements of **2**, **8**, **10**, **11** were performed in the temperature range 293–93 K in a solution of MI₁₃ (methylecyclohexane/isopentane, 1:3, by

vol.) and EPA (Et₂O/isopentane/EtOH, 5:5:2, by vol.) as solvents. The solutions with concentrations in the range from 1.0×10^{-3} to 7.0×10^{-4} M were measured between 400–220 nm in 1 cm quartz cell. Baseline correction was achieved by subtracting the spectrum of a reference solvent obtained under the same conditions. All spectra were normalized to $\Delta\epsilon$ using volume correction for EPA and MI₁₃.

The ECD solid-state spectrum of **2** was obtained using Diffused Transmission (DTCD) mode as KCl pellet placed in the integrating sphere coated with barium sulfate and introduced to the high sensitivity photomultiplier tube situated at 90 °. ECD spectrum (0.106 mg/100 mg KCl) was recorded between 400–200 nm at room temperature using the following parameters: 100 nm/min scanning speed, a step size of 0.2 nm, a bandwidth of 5 nm, a response time of 0.5 sec, and an accumulation of 5 scans. The resulting spectrum was background corrected. The KCl pellet was mounted on a rotatable holder located just before integrating sphere. The sample was measured upon rotation of the disk around the incident axis direction at various rotation angles. The spectra were almost identical, demonstrating the absence of detectable spectral artifacts. Linear dichroism (LD) was also measured, the order was less than 2×10^{-3} OD.

VCD measurements. The IR and VCD spectra of chromane **4** were measured at a resolution of 4 cm^{-1} using CDCl₃. FT-VCD spectrometer was equipped with dual sources and dual PEM's. Solution with concentration 0.17 M (8.56 mg/160 μL) was placed in a BaF₂ cell with a path length of 102 μm and assembled in rotating holder (14 sec/cycle). The ZnSe photo elastic modulator of the instrument was set to 1400 cm^{-1} . To improve the S/N ratio, the spectra were measured for 5 h 20 min (16384 scans). Baseline correction was achieved by subtracting the spectrum of a reference CDCl₃ obtained under the same conditions.

Quantum chemical calculations.

Conformational analysis and DFT optimization. The conformational search was done using HyperChem program²⁹ with MM+ force field within 5 kcal/mol energy windows, and then all structures were submitted to the Gaussian 09⁶⁹ program for DFT optimization at B3LYP/6-31G(d) level of theory. Finally, the simulated ECD spectra were calculated.

UV/ECD calculations. Simulation of UV/ECD spectra was carried out with TDDFT method for conformers found during conformational analysis. The B3LYP hybrid functional in conjunction with 6-311++G(d,p) (for **1-7**, **10**, **11**) or TZVP (for **8-11**), basis set was used. For inclusion of the solvent influence on measured ECD spectra, the polarizable continuum model (PCM) for acetonitrile implemented in the Gaussian 09⁶⁹ was used. Rotatory strengths were calculated using both length and velocity representations. The differences between the length and velocity of calculated values of rotatory strengths were <5%, and for this reason, only the velocity representations (R_{vel}) were taken into account. The ECD spectra were simulated by overlapping Gaussian functions for each transition by means of the SpecDis program.⁷⁰ The final spectra were Boltzmann averaged (T=298 K) according to the population percentages of individual conformers based on the relative Gibbs free energies (ΔG). The same results were obtained using ΔE^{SCF} and ΔH values from Gaussian output file. The calculated UV spectra were red-shifted by 5-10 nm in relation to the experiment, and consequently ECD spectra were also wavelength corrected. A Gaussian band-shape was applied with 0.25-0.38 eV as a half-height width. For demonstration of dependency between the shape of Boltzmann averaged ECD spectrum and different values of the Gaussian band-width the chromane **2** and **8** were chosen (see the Supporting Information, Figure S2 and Figure S15).

IR/VCD calculations. Computation was performed in the framework of DFT in Gaussian 09⁶⁹ package. In order to predict VCD spectra for chromane **4** first the geometry was reoptimized and then calculation of harmonic vibrational frequencies, dipole strengths and rotational strengths was carried out at the same level. B3LYP hybrid functional was tested in

conjunction with the 6-31G(d), 6-311++G(d,p) and TZVP basis sets. Comparison between theoretical and measured IR and VCD spectra were evaluated using Compare/VOA⁵⁰ confidence level algorithm. The best comparison was obtained in the case of combination B3LYP/TZVP.

ASSOCIATED CONTENT

Crystallographic data for the structure of (*S*)-Trolox methyl ester (**2**) have been deposited with the Cambridge Crystallographic Data Centre as supplementary publication no. CCDC 909503. Copies of the data can be obtained on application to CCDC, 12 Union Road, Cambridge CB2 1EZ, UK (E-mail: deposit@ccdc.cam.ac.uk).

SUPPORTING INFORMATION

The supporting information section contains a) experimental and Boltzmann averaged ECD spectra with spectra of individual conformers of compound **1**, **3-8**, and **11**; b) Cartesian coordinates for all optimized structures used throughout this work and c) crystallographic information file (CIF) for compound **2**.

ACKNOWLEDGMENTS

The authors acknowledge financial supports of the National Science Centre, Poland, grant No. N N204 177639 and grant No. G34-15 for computational time at the Interdisciplinary Center for Mathematical and Computational Modeling (ICM) of University of Warsaw, Poland.

REFERENCES

1. M. N. Chatterjea, *Textbook of Biochemistry for Dental, Nursing, Pharmacy Students* 3 edn., Jaypee Brothers Medical Publishers (P) Ltd.; 2009.
2. G. P. Ellis and I. M. Lockhart, *The Chemistry of Heterocyclic Compounds, Chromenes, Chromanones and Chromones*, Wiley-VCH, New York, 2007.
3. G. W. Burton and K. U. Ingold, *Acc. Chem. Res.*, 1986, **16**, 194-201.
4. G. W. Burton, T. Doba, E. J. Gabe, L. Hughes, F. L. Lee, L. Prasad and K. U. Ingold, *J. Am. Chem.Soc.*, 1985, **107**, 7053-7065.
5. J. A. Lucy, *Ann. N. Y. Acad. Sci.*, 1972, **203**, 4-11.

6. X. Wang and P. J. Quinn, *Progr. Lipid. Res.*, 1999, **38**, 309-336.
7. A. T. Diplock and J. A. Lucy, *FEBS Lett.*, 1973, **29**, 20.
8. J. M. Zingg, *Mol. Aspects Med.*, 2007, **28**, 481-506.
9. M. C. Aisa, C. Annetti, M. Piroddi and F. Galli, *The Encyclopedia of vitamin E*, CABI Publishing, 2006.
10. A. Azzi, R. Gysin, P. Kempna, A. Munteanu, L. Villacorta, T. Visarius and J. M. Zingg, 2004, **385**, 585-591.
11. A. Azzi, R. Gysin, P. Kempna, R. Ricciarelli, L. Villacorta, T. Visarius and J. M. Zingg, *Free Rad. Res.*, 2002, **36**, **Suppl. 1**, 30-35.
12. R. Brigelius-Flohe, *Free Rad. Biol. Med.*, 2009, **46**, 543-554.
13. J.-M. Zingg and A. Azzi, *Curr. Med. Chem.*, 2004, **11**, 1113-1133.
14. Brigelius-Flohe R and T. MG, *FASEB J.* 1999, **13**, 1145-1155.
15. Ricciarelli R, Argellati F, Pronzato MA and D. C., *Mol. Aspects Med.*, 2007, **28**, 591-606.
16. D. Enders, G. Urbanietz and G. Raabe, *SYNTHESIS* 2011, **12**, 1905-1911.
17. Y. Tang, J. Wei, W. Zhong and X. Liu, *Heteroat. Chem.*, 2010, **21**, 423-429.
18. E. Paige Stout, J. Prudhomme, K. Le Roch, C. R. Fairchild, S. G. Franzblau, W. Aalbersberg, M. E. Hay and J. Kubanek, *Bioorg. Med. Chem. Lett.*, 2010, **20**, 5662-5665.
19. S. B. Ferreira, F. de C. da Silva, A. C. Pinto, D. T. G. Gonzaga and V. F. Ferreira, *J. Heterocycl. Chem.*, 2009, **46**, 1080-1097.
20. R. H. Cichewicz, V. A. Kenyon, S. Whitman, N. M. Morales, J. F. Arguello, T. R. Holman and P. Crews, *J. Am. Chem. Soc.*, 2004, **126**, 14910-14920.
21. S. Antus, E. Baitz-Gacs, G. Snatzke and T. S. Toth, *Liebigs Ann. Chem.*, 1991, **7**, 633-641.
22. S. Antus, G. Snatzke and I. Steinke, *Liebigs Ann. Chem.*, 1983, **12**, 2247-2261

23. T. Kurtán, S. Antus and G. Pescitelli, *Electronic cd of benzene and other aromatic chromophores for determination of absolute configuration*, Comprehensive Chiroptical Spectroscopy edn., Wiley, New York, 2012.
24. F. Mazzini, M. Betti, T. Netscher, F. Galli and P. Salvadori, *Chirality*, 2009, **21**, 519-524.
25. J. M. Batista, Jr.; S. N. López, J. S. Mota, K. L. Vanzolini, Q. B. Cass, D. Rinaldo, W. Vilegas, V. S. Bolzani, M. J. Kato and M. Furlan, *Chirality*, 2009, **21**, 799-801.
26. D. Slade, D. Ferreira and J. P. J. Marais, *Phytochemistry*, 2005, **66**, 2177-2215.
27. S. Antus, T. Kurtán, L. Juhász, L. Kiss, M. Hollósi and Z. Májer, *Chirality*, 2001, **13**, 493-506.
28. F. Zhang, L. Li, S. Niu, Y. Si, L. Guo, X. Jiang and Y. Che, *J. Nat. Prod.*, 2012, **75**, 230-237.
29. J. M. Batista Jr., A. N. L. Batista, D. Rinaldo, W. Vilegas, Q. B. Cass, V. S. Bolzani, M. J. Kato, S. N. López, M. Furlan and L. A. Nafie, *Tetrahedron: Asymmetry*, 2010, **21**, 2402-2407.
30. N. J. Miller, C. A. Rice-Evans, M. J. Davies, V. Gopinathan and A. Milner, *Clin. Sci.*, 1993, **84**, 407-412.
31. J. Frelek, M. Górecki, M. Łaszcz, A. Suszczyńska, E. Vass and W. J. Szczepiek, *Chem. Comm.*, 2012, **48**, 5295-5297.
32. J. M. Batista Jr, A. N. L. Batista, M. J. Kato, V. S. Bolzani, S. N. López, L. A. Nafie and M. Furlan, *Tetrahedron Lett.*, 2012, **53**, 6051-6054.
33. J. M. Batista, A. N. L. Batista, J. S. Mota, Q. B. Cass, M. J. Kato, V. S. Bolzani, T. B. Freedman, S. N. López, M. Furlan and L. A. Nafie, *J. Org. Chem.*, 2011, **76**, 2603-2612.
34. P. Chochrek, J. Frelek, M. Kwit and J. Wicha, *J. Org. Chem.* 2009, **74**, 7300-7308
35. R. Kołodziejska, M. Górecki, J. Frelek and M. Dramiński, *Tetrahedron: Asymmetry*, 2012, **23**, 683-689.
36. P. L. Polavarapu, J. Frelek and M. Woźnica, *Tetrahedron: Asymmetry* 2011, **22**, 1720-1724.
37. K. Krohn, S. F. Kouam, G. M. Kuigoua, H. Hussain, S. Cludius-Brandt, U. Florke, T. Kurtán, G. Pescitelli, L. Di Bari, S. Draeger and B. Schulz, *Chem. Eur. J.*, 2009, **15**, 12121-12132.
38. L. Di Bari, G. Pescitelli, P. Salvadori, M. Rovini, M. Anzini, A. Cappelli and S. Vomero, *Tetrahedron: Asymmetry*, 2006, **17**, 3430-3436.
39. I. Jastrzębska, M. Górecki, J. Frelek, R. Santillan, L. Siergiejczyk and J. W. Morzycki, *J. Org. Chem.*, 2012, **77**, 11257-11269.
40. P. L. Polavarapu, *Chirality*, 2008, **20**, 664-672.
41. P. L. Polavarapu, E. A. Donahue, G. Shanmugam, G. Scalmani, E. K. Hawkins, C. Rizzo, I. Ibnusaud, G. Thomas, D. Habel and D. Sebastian, *J. Phys. Chem. A*, 2011, **115**, 5665-5673.
42. S. Witkowski, R. Anulewicz-Ostrowska and T. M. Krygowski, *Pol. J. Chem.*, 2001, **75**, 883-888.
43. K. Brzeziński, Z. Dauter, A. Baj, P. Walejko and S. Witkowski, *Acta Cryst.*, 2011, **E67**, o503-504.
44. K. Brzeziński, A. Baj, P. Walejko, S. Witkowski and Z. Dauter, *Acta Crystallographica Section E*, 2011, **67**, o1901.

45. E. V. Anslyn and D. A. Dougherty, *Modern Physical Organic Chemistry*, University Science, Sausalito, CA, 2006.
46. Y. H. Zhao, M. H. Abraham and A. M. Zissimos, *J. Org. Chem.*, 2003, **68**, 7368-7373.
47. G. Avellone, D. Bongiorno, L. Ceraulo, M. Ferrugia and V. Turco Liveri, *Inter. J. Pharm.*, 2002, **234**, 249-255.
48. A. Moscowitz, K. M. Wellman and C. Djerassi, *J. Am. Chem. Soc.*, 1963, **85**, 3515-3516.
49. G. Pescitelli, D. Padula and F. Santoro, *Phys. Chem. Chem. Phys.*, 2013, **15**, 795-802.
50. E. Debie, P. Bultinck and L. A. Nafie, *CompareVOA software*, (2010) BioTools, Inc., Jupiter, FL.
51. F. Mazzini, G. Pescitelli, L. Di Bari, T. Netscher and P. Salvadori, *Chirality*, 2009, **21**, 35-43.
52. A. Stocker, G. Derungs, W.-D. Woggon, T. Netscher, A. Rüttimann, R. K. Müller, H. Schneider and L. J. Todaro, *Helv. Chim. Acta*, 1994, **77**, 1721-1737.
53. G. Pescitelli, L. Di Bari and N. Berova, *Chem. Soc. Rev.*, 2011, **40**, 4603-4625.
54. P. Sun, D.-X. Xu, A. Mándi, T. Kurtán, T.-J. Li, B. Schulz and W. Zhang, *J. Org. Chem.*, 2013, **78**, 7030-7047.
55. P. Skowronek, J. Ścianowski and J. Gawroński, *Tetrahedron: Asymmetry*, 2006, **17**, 2408-2412.
56. S. Coriani, A. Baranowska, L. Ferrighi, C. Forzato, D. Marchesan, P. Nitti, G. Pitacco, A. Rizzo and K. Ruud, *Chirality*, 2006, **18**, 357-369.
57. D. A. Lightner and J. E. Gurst, *Organic Conformational Analysis and Stereochemistry from Circular Dichroism*, Wiley-VCH, 2000.
58. L. Huangshu and J. Atkinson, *J. Org. Chem.*, 2000, **65**, 2560-2567.
59. P. Palozza, E. Piccioni, L. Avanzi, S. Vertuani, G. Calviello and S. Manfredini, *Free Radical Biol. Med.*, 2002, **33**, 1724-1735.
60. N. Cohen, B. Schaer, G. Saucy, R. Borer, L. Todaro and A. M. Chiu, *J. Org. Chem.*, 1989, **54**, 3282-3292.
61. H. Mayer, P. Schudel, R. Ruegg and O. Isler, *Helv. Chim. Acta.*, 1963, **46**, 963-982.
62. R. West, C. Panagabko and J. Atkinson, *J. Org. Chem.*, 2010, **75**, 2883-2892.
63. C. Suarna, R. T. Dean and P. T. Southwell-Keely, *Aust. J. Chem.*, 1997, **50(12)**, 1129-1135.
64. CrysAlisPro, Agilent Technologies.
65. CrysAlisPro, Oxford Diffraction Ltd.
66. G. M. Sheldrick, *Acta Cryst.*, 1990, **A46**, 467-473.
67. G. M. Sheldrick, *SHELXL93*, (1993) University of Göttingen, Germany.
68. *International Tables for Crystallography*, Kluwer, Dordrecht, 1992.
69. M. J. T. Frisch, G. W.; Schlegel, H. B.; Scuseria, G. E.; Robb, M. A.; Cheeseman, J. R.; Scalmani, G.; Barone, V.; Mennucci, B.; Petersson, G. A.; Nakatsuji, H.; Caricato, M.; Li, X.; Hratchian, H. P.; Izmaylov, A. F.; Bloino, J.; Zheng, G.; Sonnenberg, J. L.; Hada, M.; Ehara, M.; Toyota, K.; Fukuda, R.; Hasegawa, J.; Ishida, M.; Nakajima, T.; Honda, Y.; Kitao, O.; Nakai, H.; Vreven, T.; Montgomery, J. A., Jr.; Peralta, J. E.; Ogliaro, F.; Bearpark, M.; Heyd, J. J.; Brothers, E.; Kudin, K. N.; Staroverov, V. N.; Kobayashi, R.; Normand, J.; Raghavachari, K.; Rendell, A.; Burant, J. C.; Iyengar, S. S.; Tomasi, J.; Cossi, M.; Rega, N.; Millam, J. M.; Klene, M.; Knox, J. E.; Cross, J. B.; Bakken, V.; Adamo, C.; Jaramillo, J.; Gomperts, R.; Stratmann, R. E.; Yazyev, O.; Austin, A. J.; Cammi, R.; Pomelli, C.; Ochterski, J. W.; Martin, R. L.; Morokuma, K.; Zakrzewski, V. G.; Voth, G. A.; Salvador, P.; Dannenberg, J. J.; Dapprich, S.; Daniels, A. D.; Farkas, Ö.; Foresman, J. B.; Ortiz, J. V.; Cioslowski, J.; Fox, D. J., *Gaussian 09*, (2009) Gaussian, Inc., Wallingford, CT.
70. T. Bruhn, Y. Hemberger, A. Schaumlöffel and G. Bringmann, *SpecDis*, (2012) University of Würzburg, Germany.